HHS Public Access

Author manuscript

Dev Cell. Author manuscript; available in PMC 2024 December 18.

Published in final edited form as:

Dev Cell. 2023 December 18; 58(24): 2959–2973.e7. doi:10.1016/j.devcel.2023.11.008.

A reversible epigenetic memory of inflammatory injury controls lineage plasticity and tumor initiation in the mouse pancreas

David J. Falvo[1,2], **Adrien Grimont**[1,2], **Paul Zumbo**[3,4], **William B. Fall**[1,2], **Julie L. Yang**[5], **Alexa Osterhoudt**[1,2], **Grace Pan**[1,2], **Andre F. Rendeiro**[3,6], **Yinuo Meng**[1,2], **John E. Wilkinson**[7], **Friederike Dündar**[3,4], **Olivier Elemento**[3,6], **Rhonda K. Yantiss**[8], **Erika Hissong**[8], **Richard Koche**[5], **Doron Betel**[3,4,9], **Rohit Chandwani**[1,2,10,*]

[1]Department of Surgery, Weill Cornell Medicine, New York, NY, 10065, USA

[2]Sandra and Edward Meyer Cancer Center, Weill Cornell Medicine, New York, NY, 10065, USA

[3]Institute for Computational Biomedicine, Department of Physiology, Biophysics, and Systems Biology, Weill Cornell Medicine, New York, NY, 10065, USA

[4]Applied Bioinformatics Core, Weill Cornell Medicine, New York, NY, 10065, USA

[5]Center for Epigenetics Research, Memorial Sloan Kettering Cancer Center, New York, NY, 10065, USA

[6]Caryl and Israel Englander Institute for Precision Medicine, Weill Cornell Medicine, New York, NY, 10065, USA

[7]Department of Pathology, University of Michigan, Ann Arbor, MI, 48109, USA

[8]Department of Pathology, Weill Cornell Medicine, New York, NY, 10065, USA

[9]Division of Hematology and Oncology, Department of Medicine, Weill Cornell Medicine, New York, NY, 10065, USA

[10]Department of Cell and Developmental Biology, Weill Cornell Medicine, New York, NY, 10065, USA.

SUMMARY

Inflammation is essential to the disruption of tissue homeostasis, and can destabilize the identity of lineage-committed epithelial cells. Herein we employ lineage-traced mouse models, single-cell transcriptomic and chromatin analyses, and CUT&TAG to identify an epigenetic memory of

*Lead contact: Rohit Chandwani, MD, PhD; Correspondence: roc9045@med.cornell.edu.

AUTHOR CONTRIBUTIONS

DJF designed and performed experiments, analyzed data, and wrote the paper. AG performed experiments, analyzed data, and wrote the paper. WBF, AO, GP, and YM performed experiments. PZ, JLY, AFR, FD, RKY, EH, and JEW analyzed data. OE, DB, and RK supervised data analysis. RC designed, performed, and supervised experiments, analyzed data, supervised data analysis, and wrote the paper.

DECLARATION OF INTERESTS

The authors declare no competing interests.

inflammatory injury in the pancreatic acinar cell compartment. Despite resolution of pancreatitis, our data show that acinar cells fail to return to their molecular baseline, with retention of elevated chromatin accessibility and H3K4me[1] at metaplasia genes, such that memory represents an incomplete cell fate decision. *In vivo*, we find this epigenetic memory controls lineage plasticity, with diminished metaplasia in response to a second insult but increased tumorigenesis with an oncogenic *Kras* mutation. The lowered threshold for oncogenic transformation, in turn, can be restored by blockade of MAPK signaling. Together, we define the chromatin dynamics, molecular encoding, and recall of a prolonged epigenetic memory of inflammatory injury that impacts future responses but remains reversible.

Graphical Abstract

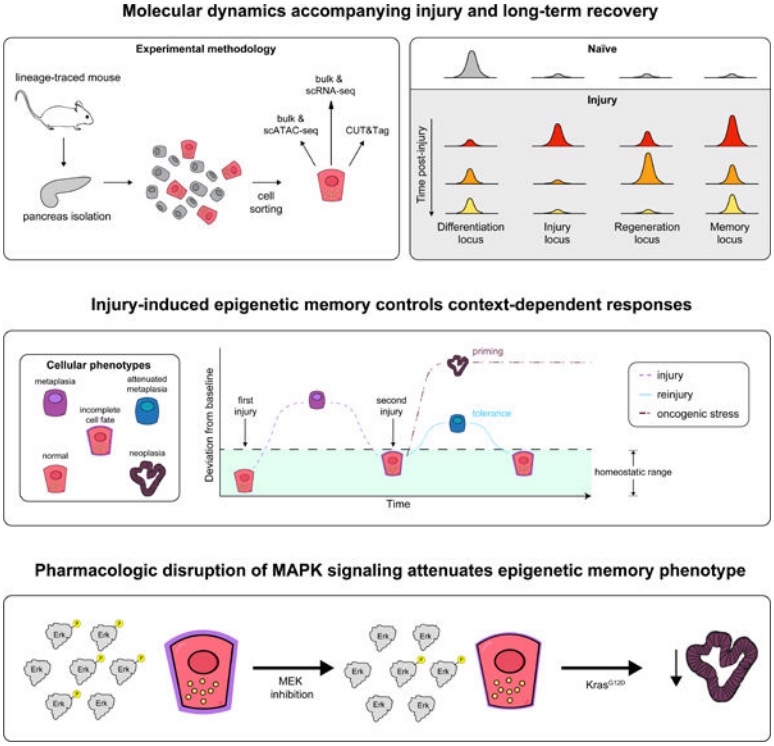

eTOC

Falvo et al. demonstrate that transient inflammatory injury leads to dynamic epigenetic alterations in lineage-committed cells of the pancreas, a subset of which are durable over time. This epigenetic memory promotes injury tolerance but lowers the threshold for tumorigenesis in a manner that invokes recall of memory and is reversible.

INTRODUCTION

Biological systems operate within fluctuating environments, and, therefore, are inherently tasked with accurately responding in real-time to a myriad of signals. Recent evidence suggests that a memory of inflammation can be encoded and retained in the epigenome of cells even following resolution of the initial stimulus.[1–4] The presence of ‘inflammatory

memory' suggests that preservation of tissue homeostasis also incorporates an evolutionary adaptation in which future responses are educated by past experiences.

In the pancreas, inflammatory injury results in a reversible cell-fate transition known as acinar-to-ductal metaplasia (ADM). Homeostasis following ADM is typically restored by prompt regeneration of the acinar compartment[5–6], given the absence of a long-lived progenitor pool in the adult pancreas.[7] By contrast, in the context of mutant *Kras*, ADM is a first step that precedes the development of pancreatic intraepithelial neoplasia (PanIN) and subsequent pancreatic ductal adenocarcinoma (PDAC). The earliest preclinical models employing oncogenic *Kras* activated by embryonic Cre drivers demonstrated sufficiency of mutant *Kras* to unveil PanIN and PDAC.[8] However, in the adult mouse, inflammation, typically experimentally elicited by the cholecystokinin analog caerulein, is necessary to give rise to neoplastic lesions that are most effectively derived from acinar cells.[9–12] Recent data highlight the capacity of inflammation to destabilize pancreatic epithelial cell identity[13–14] to promote tumor initiation via acquisition of progenitor features[5,15] and/or outgrowth of specific critical niche populations.[16] These models have thus demonstrated robust cooperativity between oncogenic stress and contemporaneous inflammation.

In the patient setting, it has been observed that chronic pancreatitis is a well-established risk factor for pancreatic cancer. Surprisingly, a single episode of self-limited acute pancreatitis is suggested to confer an increased risk of developing subsequent PDAC up to 10 years after the episode.[17] Recent evidence offers one potential explanation for this phenomenon, wherein remote inflammation can support tumorigenesis.[18] However, it remains unknown what defines chromatin domains associated with inflammatory memory, how memory evolves over time, and how it is recalled with secondary responses. Finally, whether inflammatory memory is potentially reversible is an open question.

Here, we leverage lineage tracing of pancreatic acinar cells to define the long-term ramifications of a transient inflammatory injury on pancreatic tissue homeostasis and tumorigenesis. We find that injury has a prolonged and durable impact on acinar cell identity, and this manifests as an incomplete cell fate decision. The failure to fully regenerate alters the responsiveness to a secondary inflammatory insult and to delayed activation of mutant *Kras*. Importantly, we find that the persistent molecular alterations that constitute inflammatory injury memory are amplified in secondary responses, suggesting 'recall' of the initial insult. Finally, we show that persistent low-level activation of the MAPK pathway is a feature associated with memory, and that the altered oncogenic potential in memory can be reversed via blockade of this pathway.

Our data thus highlight the ability for remote inflammatory injury to become encoded as a lasting but reversible acinar cell-specific epigenetic memory of the prior insult and to affect lineage plasticity in a context-dependent manner.

RESULTS

A transient inflammatory injury induces persistent molecular alterations following pancreatic regeneration

We first asked whether a transient inflammatory episode persistently alters the transcriptional profile and chromatin accessibility landscape of pancreatic acinar cells. We used *Mist1*-Cre^{ERT2}; CAGs-LSL-tdTomato (MT) mice to conditionally restrict tdTomato expression to the acinar compartment after tamoxifen treatment.[11] After tdTomato activation, transient inflammatory injury was induced in MT mice via intraperitoneal administration of caerulein (or saline as a control) using a 3 week protocol, followed by harvesting at either peak injury (2 days) or after a recovery interval of 3 weeks (Figure 1A). We observed that at peak injury, pancreatic histology exhibited pronounced metaplasia and tissue damage (Figure 1B). At 3 weeks of recovery, the pancreas was devoid of ADM and inflammatory infiltrates, with absence of the ductal marker CK19 from acinar cells, indicating redifferentiation of the acinar compartment (Figure 1B–C).

To assess the spectrum of molecular changes induced during and after injury, pancreata were harvested from both MT mice treated with caerulein, at 2 days and 3 weeks after the insult. tdTomato(+) acinar cells were isolated via fluorescence-activated cell sorting (FACS) for downstream profiling of transcriptional and chromatin accessibility changes using RNA-seq and ATAC-seq, respectively. At 2 days after injury (peak inflammation 2d), we observed an expected downregulation of acinar-specific genes (e.g. *Amy2b, Tff2, Cela1*), with strong upregulation of ductal (e.g. *Krt19, Onecut2)* and pro-inflammatory genes (e.g. *Ccl3, Ccl4, Cxcl2, Il1b, Tnf*). Surprisingly, we found that after 3 weeks (recovery 3w), acinar cells display a mixed transcriptional state, characterized by persistent expression of metaplasia-associated genes despite normal histology (Figure 1D). Using Gene Set Enrichment Analysis (GSEA), we observed an enrichment of transcripts involved in epithelial-to-mesenchymal transition (EMT), angiogenesis, inflammation, and related to Kras signaling at 3 weeks of recovery suggesting incomplete regeneration at this timepoint (Figure 1E; Figure S1A).

Next, we evaluated the changes in chromatin accessibility at the peak of injury and after resolution of pancreatitis. Principal Component Analysis (PCA) on the ATAC-seq data from FACS-sorted acinar cells showed separation between peak injury and recovery 3w mice; consistent with the RNA-seq data, chromatin accessibility remained altered from baseline after 3 weeks of recovery (Figure S1B). Injury-exposed tdTomato(+) acinar cells exhibited dramatically reduced accessibility at genomic regions enriched in control acinar cells (Figure 1F; Cluster 1), suggesting a loss of acinar cell identity. Additionally, we observed profound gains in accessibility at intergenic and intronic regions unveiled during peak injury (Figure 1F; Clusters 3 and 4). Interestingly, we found that there were continued gains of accessibility at 3 weeks of recovery (Figure 1F; Cluster 2) despite resolution of gains in Cluster 4, highlighting ongoing molecular changes in the acinar compartment despite evidence of regeneration by histology. Whereas the majority of persistent transcriptional changes at 3 weeks were a subset of the ‘peak inflammation 2d’ differentially expressed genes (DEGs), the differentially-accessible regions (DARs) specific to 3 weeks of recovery

were greater in number and more distinct (Figure 1G). This suggests that chromatin remains highly dynamic up to 3 weeks after a transient insult.

Next, we performed motif analysis on the clustered DARs, identifying a number of acinar-specific factors (e.g. Ptf1a, Bhlha15) in Cluster 2, while motifs for factors involved in pancreatitis were found in Cluster 4 (e.g. AP-1, Nr5a2) (Figure 1H; Figure S1C). Broadly, 3 weeks of recovery restored accessibility of regions enriched in motifs for lineage-specifying TFs (Nr5a2, Bhlha15, Nkx6.1) but showed persistent depression of AP-1 motifs (Figure S1D). Gene Ontology (GO) enrichment analysis on the clustered DARs identified a number of processes associated with the extracellular matrix (ECM) in Cluster 2 (Figure 1I), suggesting that there are ongoing changes in tissue architecture at 3 weeks of recovery). In Cluster 4, where there are transient increases in accessibility, we found GO terms associated with pancreatitis (e.g. immune system process, exocytosis). Acinar cells thus retain expression of genes upregulated during pancreatitis and accumulate clear gains in accessibility at sites normally absent in control acinar cells, while also failing to re-establish baseline accessibility at acinar-specific locations.

An epigenetic memory of inflammatory injury is durable over time

Because we observed emergent acinar cell chromatin alterations at 3 weeks following pancreatitis, we asked how these molecular dynamics evolve over time. At 12 and 18 weeks of recovery, we saw continued evidence of normal tissue architecture (Figure 2A), and no persistent changes to the abundance of the ADM/ductal markers Sox9 and CK19 (Figure S2A–B) nor the acinar marker Cpa1 (Figure S2B). We evaluated the persistence of the progenitor markers Klf5 and Nestin; while these were robustly induced at peak injury, there was no lasting expression at 12 weeks (Figure 2B).

We then asked if there was a persistent microenvironment change that accompanied the recovery from pancreatitis. Single-cell RNA-sequencing on the entire pancreas at peak injury showed emergence of a metaplastic population after caerulein, accompanied by increases in fibroblasts and macrophages (Figure S2C–D). However, after 12 weeks, we saw no persistent immune infiltrate nor a shift in transcriptional state among immune cells, fibroblasts, or endothelial cells (Figure S2C–D). We did observe an increase in T cells 12 weeks after pancreatitis in our scRNA-seq, but orthogonal profiling of the immune compartment via flow cytometry could not confirm this across many replicate mice (Figure 2C). Immunophenotyping also confirmed the scRNA-seq findings of robust infiltrates of macrophages and monocytes at 2 days that returned to baseline levels with 3 and 12 weeks of recovery. No accumulation of dendritic cells or B cells was evident (Figure 2C). By immunofluorescence, we also saw no evidence at 12 weeks of residual infiltration of macrophages and T cells by F4/80 and CD3 staining, respectively (Figure 2D). These data thus suggest that there are no apparent stable perturbations to cell type composition 12 weeks after pancreatitis.

Our data therefore suggested a restoration of tissue architecture, gene expression, and microenvironment composition with prolonged recovery. Next, we determined if chromatin alterations in acinar cells persist despite these findings. Unexpectedly, we found that even after 18 weeks of recovery, acinar cells retained a chromatin signature of prior injury

(Figure 2E; Cluster 3 [memory]). Motif enrichment of these gained memory regions showed an abundance of AP-1 motifs, with a top gene ontology (GO) term corresponding to MAPK pathway (Figure 2F). Conversely, acinar cell identity regions in Cluster 1 failed to completely restore chromatin accessibility enriched in controls, even after 12 and 18 weeks of recovery. We found that the sites in Cluster 1 (acinar-identity) were enriched for ETS factor and Sox17 motifs, known to be involved in pancreas development, and identified GO terms associated with processes important for acinar cell function (i.e. zymogen binding) (Figure 2F). Interestingly, regions enriched in Cluster 2 that initially increased accessibility up to 3 weeks of recovery were markedly lost at 6 weeks of recovery and beyond, suggesting that the full range of chromatin dynamics are more adequately revealed with prolonged recovery (Figure 2E). Together, these data highlight a prolonged cell-intrinsic effect of prior injury on chromatin states that is not manifested histologically.

To define statistically the presence of an acinar cell-specific memory of inflammatory injury, we employed ELBOW, ranking peaks induced at peak injury by their 12 weeks / control DESeq2 Wald statistic.[19] Using ELBOW, we identified 3546 peaks as ‘persistent’ (Figure 2G), with the bulk of these colocalizing with distal intergenic and intronic regions – i.e. enhancers (Figure 2H). By contrast, promoters with dynamic accessibility over time tended to be much more frequently ‘resolved’ or ‘suppressed’, indicating that genes with inducible accessibility were much more likely to either lose the increased ‘openness’ or become ‘closed’, respectively, over time. In other words, we observed that enhancers, not promoters, are the principal component of memory (Figure 2I).

To contextualize our findings with respect to prior work, we analyzed our memory domains in cluster 3 against prior reports of chromatin unveiled in caerulein-mediated injury.[14,18] Importantly, we found that our memory domains overlapped highly with chromatin identified previously as being common to injury and neoplasia (‘shared injury-neoplasia peaks’) (Figure S2E) and much less so with chromatin specific to injury (‘injury-associated peaks’) (Alonso-Curbelo et al, 2021). We also found that our memory domains did not overlap highly with those found at day 28 after acute pancreatitis (Del Poggetto et al, 2021); instead these ‘memory (ctrl vs. D28) peaks’ were far more shared with our cluster 2 (‘regeneration’) peaks, a group of peaks not found beyond 3 weeks following subacute pancreatitis, and ones that we do not observe as being persistent over time. Cluster 3 thus defines a set of memory domains that are not only durable but are also found in Kras-driven neoplasia, highlighting the possibility of a role for this prolonged memory in tumorigenesis.

Persistent retention of H3K4me^1 is a feature of memory chromatin

We then sought to articulate the dynamic histone modifications associated with inflammatory injury and memory of this insult. Using Cleavage Under Targets and Tagmentation (CUT&TAG) on sorted acinar cells from control (‘saline 2d’) and peak injury (‘caerulein 2d’), we evaluated genome-wide occupancy of H3K4me^1 (all enhancers), H3K27ac (active promoters and enhancers), and H3K27me^3 (repressed promoters and enhancers). Genome-wide, we found robust differences across all three marks induced by peak injury. Inflammatory injury induced the deposition of both active H3K27ac and repressive H3K27me^3 throughout the genome, while dynamic H3K4me^1 had an equal

distribution of gains and losses in abundance in chromatin (Figure S3A). When we evaluated histone modifications in the context of DARs, cluster 1 (acinar-identity) regions were notable for decreased H3K27ac but not H3K4me^1 following injury. Conversely, injury induced increases in H3K4me^1 in clusters 2 (regeneration), 3 (memory), and 4 (inflammation-associated) peaks; H3K27ac, interestingly, only showed robust increases at peak injury in the cluster 3 (memory) peaks, but not the other increased accessibility ('regeneration' and 'inflammation-associated') clusters (Figure 3A).

We then evaluated whether any of the alterations to H3K4me^1, H3K27ac, or H3K27me^3 persisted over time in ELBOW-defined 'persistent', 'resolved', 'suppressed' and 'unchanged' DARs. At 12 weeks following the inflammatory insult, we found that the high levels of H3K27ac induced at peak injury in 'persistent' peaks are lost. Broadly, we saw that H3K27ac levels returned to baseline in all ELBOW-defined categories (Figure 3B). By contrast, H3K4me^1 showed evidence of retention specifically at 'persistent' regions (Figure 3B), including distinct enhancers at the *Runx1* and *Fam107b* loci (Figure 3C). As an orthogonal method, we performed ELBOW analysis on induced H3K4me^1 and H3K27ac, identifying in a statistical unbiased manner that of the peaks gained in the initial response to injury, 36% and 18%, respectively, are persistent over time (Figure S3B–C). Together, these data suggest that the primary chromatin signature of cell-type specific memory of inflammatory injury is of increased accessibility in conjunction with persistent H3K4me^1, as has been described in the skin[19] and macrophages[2].

Memory of inflammatory injury manifests as an 'incomplete cell fate decision'

To determine if any persistent transcriptional changes accompanied the chromatin dynamics, we performed bulk RNA-seq to specifically interrogate sorted tdTomato(+) acinar cells. We found a subtle shift in clustering of caerulein + 12 week recovery ('prior inflammation') samples versus saline + 12 week recovery ('naïve') samples (Figure 3D). Few statistically significant individual gene expression changes were found at this timepoint (Figure S3D), with only nine genes differentially expressed. However, at the pathway level, there were increases in both inflammatory and metaplasia-specific (ADM) transcripts[20] in prior injury samples; conversely, acinar transcripts[20] were enriched in naïve acinar cells (Figure 3E–G). Further, leading-edge ADM genes increased in expression in prior injury displayed nearby regulatory elements with persistently increased accessibility (i.e. cluster 3 (memory)-type), while acinar gene-related enhancers exhibited cluster 1 dynamics (as in Figure 2I).

Leveraging our single-cell RNA-seq data, we asked if individual cells show residual metaplastic gene expression. We focused on the epithelial compartment across the temporal resolution of injury (Figure S3E), identifying clusters 3 and 9 as being enriched in the initial response to injury. Indeed, these cells showed coexpression of Cpa1 and CK19, indicating that these emergent cells in peak injury were bona fide ADM cells (Figure S3F). We then quantified ADM cells (clusters 3 + 9) over time, finding a robust increase in their number with injury (13% in caerulein-treated versus 1% in control) and persistence of these transcriptional states over time (9.1% in caerulein 12w versus 4.9% in saline 12w) (Figure S3G). In the memory state, clusters 3 and 9 were transcriptionally enriched for Egr1, Reg3a, Reg3b, and several AP-1 transcription factors (Jun, Fos, Atf3, Fosb, Jund), whilst relatively

depleted of the acinar enzyme transcripts Cela1, Try10, and Cpb10. These results suggest that injury establishes a memory of inflammatory injury that manifests as an incomplete cell fate decision (defined by the persistence of cluster 3 and 9 cells that have a highly mixed cellular identity). Both bulk chromatin accessibility and transcriptional states reinforce the notion of an incomplete cell fate decision, with residual subtle evidence of the remote metaplastic event in a subpopulation of epithelial cells.

Prior inflammatory injury diminishes the capacity for subsequent metaplasia

Given these findings, we asked whether the memory of injury impacts acinar cell responses to future stimuli. We first tested if after 12 weeks of recovery from subacute pancreatitis the capacity to undergo metaplasia is altered (Figure 4A). Surprisingly, pancreata exposed to prior injury are refractory to secondary acute inflammatory rechallenge, with increased ADM in naïve mice compared to injury-resolved mice at 2 days (Figure 4B–C) and through resolution at 7 days (Figure 4C). Co-staining of Cpa1 and CK19 was observed in injury-resolved tissue re-challenged with caerulein, indicative of early ADM, while Cpa1 was lost in the metaplastic lesions of injury-naïve tissue similarly re-challenged, suggesting more advanced ADM (Figure 4D). Interestingly, the degree of CK19 positivity was not overall different between naïve and rechallenged mice, despite the clear differences in histology. In addition, cleaved-caspase 3 (CC3) staining co-localized with advanced metaplastic lesions, was proportional to the degree of metaplasia, and was not otherwise differentially enriched depending on the prior insult (Figure 4E). We performed similar *in vivo* re-challenge experiments with fewer caerulein injections to determine if our findings were robust to changes in the degree of secondary insult. Again, we observed more metaplasia in naïve pancreata as compared to rechallenged pancreata (Figure S4A–B), findings that were in contrast to previous reports.[18]

We asked if the initial insult with a subacute pancreatitis over 3 weeks drove ‘tolerance’ in a manner specific to this caerulein schedule. To address this, we instead used acute pancreatitis (AP; 16 hourly injections over 2 days) as in prior reports[18] followed by 4 weeks of recovery and re-challenge with acute inflammatory rechallenge (Figure S4C). Once again, we found that prior injury did not increase the frequency of metaplasia across multiple mouse cohorts (Figure S4D), irrespective of whether or not mice were starved for 24 hours prior to the secondary insult (Figure S4E). Using a 12 week window between primary and secondary AP (Figure S4F), we observed that prior injury protected against metaplasia upon rechallenge, regardless of whether mice were starved (Figure S4G–I). Therefore, prior inflammatory injury was associated with diminished lineage plasticity and enhanced tolerance to further insults, regardless of pancreatitis protocol and the degree of initial injury.

To further understand the phenotypic consequences of inflammatory memory, we tested if prior injury alters the capacity of acinar cells to transdifferentiate *in vitro* in a cell-autonomous fashion. We exposed wild-type C57BL/6 mice to primary injury (or control) followed by a recovery period of 12 weeks, and isolated acinar cells for embedding in Matrigel (Figure 4F). In the absence of rhTGFα, we observed no change in acinar cells from naïve or prior injury mice (Figure 4G, upper panels). Treatment with rhTGFα *in vitro*, which activates signaling downstream of EGFR, gave rise to ductal cystic structures (Figure 4G,

lower panels), a process that mimics ADM.[5,21] Unexpectedly, injury-resolved acinar cells generated substantially larger cystic structures when compared to injury-naïve acinar cells (Figure 4H). The impact of prior injury is thus to diminish metaplastic lesions *in vivo* in response to caerulein but the mitogenic effect of growth factors is elevated.

These seemingly contradictory results raised the question of why we observed discordant metaplastic responses between *in vitro* and *in vivo* systems. Given the degree of overlap between signaling downstream of the CCK receptor and EGFR, we reasoned that there might be a persistent change in upstream receptor abundance. Immunoblotting in lysates from naïve or prior injury mice 12 weeks after caerulein showed decreased Cckar and elevated phosphorylated Erk in mice long after caerulein insult (Figure 4I–J). These findings reinforce the notion that metaplastic cells do not fully recover from the initial pancreatitis episode and offer a mechanistic explanation for why acinar cells with memory respond less to caerulein but more to specific activation of MAPK signaling.

Prior inflammatory injury lowers the threshold for subsequent Kras-driven tumor initiation

We reasoned that several features of memory - the heightened response to a specific EGFR ligand *in vitro*, persistent elevation of phospho-Erk, retention of accessibility at MAPK-related enhancers found also in neoplasia, and enrichment for metaplastic gene expression -- would imply that prior exposure to injury lowers the threshold for neoplastic transformation. To test this, we treated MT and *Mist1*-Cre^{ERT2}; LSL-Kras$^{G12D/+}$; CAGs-LSL-tdTomato (MKT) mice with either saline or caerulein as before, followed by 3 weeks of recovery, and then activation of Kras^{G12D} with tamoxifen (Figure S5A). Importantly, this system provided complete temporal control over endogenous levels of *Kras* expression and with specific restriction to pancreatic acinar lineage, complementing older studies using prolonged pancreatitis (90 days) followed by Kras^{G12V} activation[10] and recent studies using the inducible *Kras* (iKras) model that is exocrine-specific and features mild overexpression of mutant *Kras*.[18] With 3 weeks of recovery between injury and *Kras*^{G12D} activation, we observed substantial PanIN development in mice recovered from prior injury, as compared to rare lesions in naïve mice (Figure S5B). Extension of the temporal separation to 12 weeks (Figure 5A) showed increased ADM and PanIN in prior injury mice (Figure 5B–C). Immunofluorescent staining of both naïve + *Kras*^{G12D} and prior injury + *Kras*^{G12D} pancreas sections revealed the loss of Cpa1 and accumulation of CK19 in these PanIN lesions (Figure 5D; Figure S5C). We also found that the PanIN lesions were identifiable by Alcian blue staining (Figure 5E) and were enriched with Dclk1^{+} cells[16], but not to different degrees between comparable lesions in the two conditions (Figure S5D).

To evaluate the synergistic limits of inflammatory memory combined with oncogenic Kras we then restricted the duration of Kras^{G12D} activation to a brief window of 2 days (Figure S5E). Surprisingly, even short-term activation of Kras^{G12D} was sufficient to induce neoplastic transformation in injury-exposed acinar cells; pancreata of naïve mice were devoid of any PanIN, and displayed only sparse early metaplastic lesions (Figure S5F–G). Indeed, CK19+ Cpa1- lesions (Figure S5H) and Dclk1+ lesions (Figure S5I) were found only in the context of prior injury. These findings indicate differential responses to oncogenic *Kras* in the presence or absence of a temporally remote prior inflammatory injury.

Neoplastic transformation is associated with recall of epigenetic memory

To understand the molecular underpinnings of this phenotype, we performed RNA-seq on naïve and prior injury tdTomato(+) acinar cells subjected to brief *Kras*^{G12D} activation. Transcripts associated with PanIN and proliferation were specifically upregulated in mice with prior exposure to injury despite both cohorts having the same duration of *Kras* activation (Figure 6A). Despite relatively few transcriptional differences prior to *Kras* activation, naïve and prior injury samples diverged after mutant *Kras*, with >2000 DEGs. DEGs between prior injury and naive conditions (both with superimposed *Kras*^{G12D}) were more likely to be associated with cluster 3 (memory) DARs than any other cluster (Figure 6B). Additionally, we found that the leading-edge ADM transcripts that define the transcriptional component of memory (see Figure 3G; 'ADM primed') were more likely to be differentially expressed between prior injury and naive mice in the context of brief *Kras*^{G12D} activation (Figure 6C). Unexpectedly, the leading-edge acinar transcripts slightly diminished in samples exposed to prior injury (see Figure 3G; 'acinar primed') were not further downregulated upon brief activation of Kras^{G12D} (Figure 6C). Among the most differentially expressed genes between prior injury + *Kras*^{G12D} and naive + *Kras*^{G12D} conditions were the PanIN transcripts *Pgc, Krt7*, *Gkn2*, and *Gkn3,* all of which have nearby putative enhancers displaying increased accessibility long after prior injury (i.e. cluster 3-type) (Figure S6A; as in Figure 2I). These findings suggest that the memory of prior inflammatory injury is recalled in the response to delayed *Kras*^{G12D} activation, with both primed transcripts and chromatin unveiled with oncogene activation.

To further validate these findings, we performed scATAC-seq in mice treated with saline or caerulein followed by 12w recovery, before and after 2 days of mutant *Kras* activation. In the entire pancreas, we observed that prior injury + *Kras*^{G12D} was associated an influx of fibroblasts and immune cells, in keeping with the emergence of neoplastic lesions (Figure 6D). Focusing on DARs in the acinar compartment, we were able to detect seven clusters of cells, with a population reflecting PanIN cells only seen in the prior injury + *Kras*^{G12D} condition (Figure 6E; C1). We also found further evidence of memory, with cells from prior injury mice displaying much higher numbers of C7 cells and fewer C6 cells both before and after *Kras* activation (Figure 6F), affirming the bulk ATAC-seq data. Indeed, C7 cells enriched in memory were closely related to cells emerging after *Kras* in C1, and both C1 and C7 were most enriched for regions in (cluster 3) memory chromatin (Figure S6B). By contrast, C6, largely absent in the post-injury state, was enriched for (acinar-identity) cluster 1 chromatin (Figure S6B). Together, these single-cell data confirm that the molecular alterations induced by mutant *Kras* in injury-resolved mice are closely linked to the transcriptomic and chromatin features that constitute memory.

MAPK pathway inhibition reverses the effect of memory to potentiate tumor initiation

Because of the durability of memory and the recall of memory with mutant *Kras*, we hypothesized that a therapeutic opportunity to alter the lowered threshold for neoplastic transformation could be present in the 12 week window between injury and *Kras* activation. To test this, we treated MKT mice with caerulein, followed by 12 weeks of recovery during which we administered a MEK inhibitor, followed by washout prior to activation of mutant *Kras* (Figure 6G). Trametinib-treated mice displayed decreased ADM and PanIN (Figure

6H), a finding that was significant across several mice (Figure 6H; Figure S6C). Importantly, trametinib administration for 4 weeks prior to *Kras*^{G12D} activation and concurrent caerulein showed no impact on the development of ADM or PanIN (Figure 6H; Figure S6C), highlighting that pre-treatment with MEKi does not itself affect lineage plasticity except in the context of a memory of injury that perturbs cell fate (Figure S6D). These data demonstrate that the lowered threshold for tumor initiation can be reversed by targeting the specific molecular features of acinar cell memory.

DISCUSSION

To maintain tissue homeostasis, resident cells must engage in a vast array of choreographed molecular adaptations to endure an array of unforeseen events. These adaptations, often encoded as an epigenetic memory, in turn affect how tissues respond over time to secondary insults.[1–4,18] Most frequently, epigenetic memory has been associated with the response to inflammation. In the pancreas, inflammation drives the infiltration of macrophages[22–23], fibroblasts[24], and T cell subsets[25], that together control cell-intrinsic alterations in acinar cell fate wherein they acquire duct-like features[26] and dedifferentiated programs[5,15]. However, in the absence of mutant *Kras*, acinar-ductal metaplasia elicited by inflammatory injury is followed by regeneration of the acinar compartment. Here we demonstrate that this regeneration is incomplete. Specifically, inflammatory injury leads to the generation of a durable lineage-specific epigenetic memory in the pancreatic acinar cell. We find this memory is molecularly encoded as an incomplete regeneration following acinar-ductal metaplasia and is recalled in divergent cell fate decisions following re-challenge with severe injury or oncogenic stress.

Similar findings have recently been reported[18], wherein delayed activation of mutant *Kras* (using the doxycycline-inducible iKras model) in pancreatic epithelial cells was shown to lead to shorter survival in mice recovered from a transient inflammatory insult. In epithelial cells, the authors found broad increases in chromatin accessibility 28 days after acute pancreatitis. By extending our molecular analyses out to 18 weeks after pancreatitis, we find evidence of time-dependent resolution of initial broad gains in chromatin accessibility and near-complete resolution of transcriptional changes. We show that (1) chromatin defining acinar identity is acutely lost, and regained slowly over time; (2) specific regions are only opened briefly at the peak of injury; (3) regeneration features a distinct set of regulatory elements that are unveiled specifically in the first few weeks after injury; and (4) a ‘retained memory’ of inflammatory injury is not a gradual accumulation of chromatin accessibility, but instead a failure to resolve completely the changes that occurred in the initial insult. Importantly, the chromatin that accumulates accessibility in the first few weeks does not represent the durable memory, but is instead the subset of enhancers most dynamic in H3K27ac that retains H3K4me^{1}.

Recent work providing evidence of inflammatory memory has either been restricted to the stem cell compartment or not specific to a single lineage-committed cell type. Here we demonstrate by tracing the adult acinar cell that an epigenetic memory of injury is an incomplete cell fate decision, wherein ADM chromatin features are partially retained (e.g., cluster 3 memory domains, ADM transcripts), certain acinar features are lost (e.g.,

cluster 1 acinar-identity domains, acinar transcripts), and MAPK signaling is altered. This incomplete cell fate decision can be directly measured as a subset of cells retaining metaplasia-associated molecular alterations. Indeed, findings in other tissues suggest that differentiated cells in the colon or stem cells in the epidermis retain a memory of their embryonic[27] or niche[28] origins, respectively. Together, our data provide concrete evidence that transient cell fate decisions also can be encoded as an epigenetic memory.

Prior studies support a role for inflammatory memory in driving subsequent responses. In recent studies, rechallenge with caerulein after a 28 day recovery period following acute pancreatitis was associated with increased metaplasia but limited tissue damage.[18] Surprisingly, we find that regardless of the caerulein schedule or recovery interval (4 weeks or 12 weeks), prior injury limits ADM in response to secondary injury. This suggests a homeostatic adaptation, namely the downregulation of the CCK receptor, that does not require metaplasia to resist tissue-level injury. Indeed, in the human setting, it is well-known that repeated episodes of pancreatitis elicit progressively decreased release of amylase in the serum. We thus conclude that prior injury thus serves not only to drive lineage plasticity, but can also restrain responses. Further understanding of the molecular mechanisms that allow for acinar cells to ‘tolerate’ a second inflammatory injury warrant further study, and highlight that ADM is not purely a precursor to pancreatic neoplasia but instead a high-plasticity cell state from which tumors can emerge[15].

Importantly, inflammatory memory in the pancreas appears to support *Kras*-driven pancreatic tumorigenesis. The iKras model system utilized recently closely recapitulates human PDAC but features overexpression of $Kras^{G12D}$, requiring neither injury nor genetically defined tumor suppressor inactivation for progression to malignancy.[29–30] As such, the question of whether injury supports the progression of nascent tumors or initial lineage plasticity remains unclear. The model utilized herein restricts to the acinar lineage using the Mist1-Cre^{ERT2} allele, which does not invoke haploinsufficiency of a critical acinar identity TF, as occurs in mice using Ptf1a-Cre that have been used previously. We also limit mutant *Kras* expression to endogenous levels and activation only in the adult mouse, such that injury is required for the loss of acinar cell identity[9,14] and the model more faithfully recapitulates tumor initiation in human disease. Because of these genetic considerations, control animals display only rare PanIN development, such that we are able to detect that it is lineage plasticity that is affected by inflammatory memory and not more facile progression following initial ADM or PanIN formation. Inflammatory memory thus potentiates acquisition of neoplastic cell fate, and surprisingly can serve as a substitute for contemporaneous injury in contexts where the latter is essential.[14]

In the nervous system, an essential feature of memory is recall; absent memory recall, the findings that we observe could simply represent a persistent change that is unrelated to subsequent cellular responses. Here we show that mutant *Kras* activation after memory consists of enhanced transcription of specific memory-associated transcripts as well as genes associated with memory chromatin. Molecular interrogation of memory reveals the MAPK pathway, critical to both metaplastic and regenerative components of the response to injury[31], as derepressed in memory. Indeed, administration of a MEK inhibitor in the window between temporally separated caerulein and mutant *Kras* activation drives a

reduction in neoplastic transformation. Whether such means can be leveraged in other epigenetic memory contexts or in the patient setting is a potentially robust area of future inquiry.

Taken together, our data demonstrate that transcriptional and epigenetic reprogramming in response to an inflammatory injury yields persistent alterations to the pancreatic acinar cell; in turn, those precise injury-induced alterations are amplified with secondary and substantially delayed oncogenic stress. How this memory is propagated and its specific encoding in chromatin beyond accessibility remain open questions. We and others have demonstrated roles for AP-1 components in defining 'memory' chromatin[3,4,32–33], but closer analyses of TF engagement or at key regulatory elements that define memory warrant further study. Specifically, AP-1 has been recently proposed as a universal mediator of memory[19], but the cognate TFs that confer context-specificity to each lineage / response pair are still to be elucidated. Overall, our findings identify inflammatory memory as driving lineage plasticity in early neoplastic cell fate decisions, and offer insights into the induction of epigenetic 'amnesia' of an inflammatory insult as a potentially broad cancer prevention strategy.

Limitations of the study:

Here we examined memory in one cell type of the pancreas in the context of a single form of injury; whether these findings are generalizable across multiple forms of injury to the pancreas and to other differentiated cell types is a limitation of the study. Finally, how the acinar-specific memory affects crosstalk with other cell types has not been explored fully in this study.

STAR METHODS

Resource availability

Lead contact.—Further information and requests for resources and reagents should be directed to and will be fulfilled by the lead contact, Rohit Chandwani (roc9045@med.cornell.edu).

Materials availability—This study did not generate new unique reagents.

Data and code availability—All high-throughput sequencing data, both raw and processed files, have been deposited in NCBI's Gene Expression Omnibus and are publicly available. Accession numbers are listed in the key resources table. Microscopy data reported in this paper will be shared by the lead contact upon request.

This paper does not report original code.

Any additional information required to reanalyze the data reported in this paper is available from the lead contact upon request.

Experimental model and study participant details

Animal models.—Mice were housed in a pathogen-free facility at Weill Cornell Medicine (WCM) under standard housing conditions. All manipulations were performed under the Institutional Animal Care and Use Committee (IACUC)–approved protocol (2017–0038). Mouse lines used were described previously: Mist1-Cre^{ERT2} (MGI:3821734 Bhlha15$^{tm3(cre/ERT2)Skz}$)[11], LSL-Kras^{G12D} (MGI:2429948 Kras^{tm4Tyj})[34–35], LSL-tdTomato (MGI:3809523 Gt(ROSA)26Sor$^{tm9(CAG-tdTomato)Hze}$)[36]. Male and female animals were used for experiments and mice of the same sex were randomly assigned to experimental groups. Mist1:Cre^{ERT2}, LSL-Kras^{G12D}, CAGs-LSL-tdTomato mice were bred to generate Mist1-Cre^{ERT2}; LSL-Kras^{G12D}; LSL-tdTomato mice, referred to as MKT mice. Mice without Kras^{G12D} are referred to as MT mice.

Primary acinar cell culture.—Acinar 3D culture were generated as described (Shi et al., 2015) with few modifications. Briefly, acinar cell isolation was obtained with collagenase/dispase mix dissociation as described below, then cells were filtered through a 100 μm cell strainer.

Method details

Tamoxifen treatment.—Tamoxifen (Sigma) was dissolved in corn oil and administered by subcutaneous injections (at the indicated ages) at a dosage of 5 mg per injection. Mice were injected once a day for a total of 3 days—administered every other day (total duration: 5 days). Mice were allowed to recover 1 week after the last Tamoxifen treatment before receiving other treatments (if required).

Experimental pancreatitis.—For acute pancreatitis treatment, mice received 8 hourly intraperitoneal (IP) injections over two consecutive days of either PBS (saline) or caerulein at a dosage of 75 μg/kg diluted in sterile PBS. For the subacute pancreatitis protocol, mice were treated with three hourly IP injections a day, three times a week for three weeks; for the abbreviated acute pancreatitis protocol, mice were treated with five hourly injections in a single day, as indicated. For each experiment, pancreata or a portion of pancreata were harvested for histologic analysis.

Mouse pancreatic dissociation.—Mice were euthanized using CO_2, and pancreata were excised and placed in 3 mL of ice-cold HBSS while the subsequent pancreata were being harvested. Then, the ice-cold HBSS solution was discarded and pancreata were placed in a 10 cm dish, containing 5 mL of 37°C collagenase and dispase (CD) mix solution—collagenase D is used for normal tissue; collagenase V is used for fibrotic tissue (CD; ingredients: HBSS w/ Ca2+ Mg2+, Collagenase D / V [1 mg/mL], Dispase II [2 U/mL], STI [0.1 mg/mL], DNase I [0.1 mg/mL]). Pancreata were mechanically dissociated into ~1–3 mm pieces using razor blades while in CD solution. Minced pancreata were then transferred to 50 mL conical, and an additional 5 mL of CD solution were added, bringing each sample to a final volume of 10 mL. Tubes were placed on a 37°C orbital shaker at 135 rpm for 30 minutes. After incubation, the samples were centrifuged at 1000 rpm for 3 mins, washed with PBS, and then resuspended and incubated with 2 mL of 0.05% Trypsin-EDTA (37°C) for less than 2 min. Trypsin was inactivated immediately after incubation with 10

mL of 37°C PBS/FBS solution (ingredients: PBS w/o Ca2+ Mg2+, FBS [1:5], STI [0.1 mg/mL], DNase I [0.1 mg/mL]). Each tube was then gently inverted twice, centrifuged and resuspended in 10 mL of 37°C FACS buffer (ingredients: PBS, EGTA [10mM], FBS [2%], STI [0.1 mg/mL], DNase I [0.1 mg/mL]). Cell suspension was passed through a 100 μm mesh filter into a new 50 mL conical tube, centrifuged, resuspended with 1 mL of FACS buffer solution with DAPI staining [1:100] and finally transferred to a 40 μm FACS filter tube. All samples were kept on ice before and after FACS. For all FACS, Becton-Dickinson Influx or Becton-Dickinson Aria II were used to collect DAPI-/tdTomato+ cells.

Bulk RNA-seq.—Following mouse pancreas dissociation, DAPI-/tdTomato+ cells were FACS-sorted directly into TRIzol (100k cells per 750 mL TRIzol) in 1.5 mL microcentrifuge tube. Guanidinium thiocyanate-phenol-chloroform extraction was performed directly and the quality of the samples was determined using the Agilent RNA 6000 Nano Kit on the Agilent Bioanalyzer (Weill Cornell Medicine Genomics Resources Core Facility; WCM-GRCF). The WCM-GRCF prepared libraries using TruSeq RNA Sample Preparation (Non-Stranded and Poly-A selection), and used the NovaSeq 6000 (S1 Flow Cell – Paired End 2x50 cycles) for sequencing. The sequences were aligned to the mouse reference genome (mm9) using STAR[37], a universal RNAseq aligner. To improve accuracy of the mapping, the genome was created with a splice junction database based on Gencode vM1 annotation.[38] Sequences that mapped to more than one locus were excluded from downstream analysis, since they cannot be confidently assigned. Uniquely mapped sequences were intersected with composite gene models from Gencode vM1 basic annotation using featureCounts[39], a tool for assigning sequence reads to genomic features. Composite gene models for each gene consisted of the union of exons of all transcript isoforms of that gene. Uniquely mapped reads that unambiguously overlapped with no more than one Gencode composite gene model were counted for that gene model; the remaining reads were discarded. The counts for each gene model correspond to gene expression values, and were used for subsequent analyses. Prior to the detection of differentially expressed genes, the quality of the sequences was assessed based on several metrics using FastQC and QoRTs.[40–41] Differential gene expression analysis was performed for each comparison using limma voom with default parameters.[42]

Bulk ATAC-seq.—Following pancreas cell isolation, 50k DAPI-/tdTomato+ acinar cells were sorted into FACS buffer supplemented with FBS [1:10] and ATAC performed as per Buenrostro and colleagues.[43] Briefly, acinar cells were centrifuged at 500g for 5 minutes (4°C) and washed with 50 μL of cold PBS. Cells were subsequently lysed using cold lysis buffer and immediately spun at 500g for 10 min (4°C). Pellet was resuspended in the transposase reaction mix for the Tn5 tagmentation step for 30 minutes at 37°C and sample was purified using a Qiagen MinElute PCR Purification Kit. Next, DNA was indexed and amplified using PCR. The quality of the samples was assessed using Agilent High Sensitivity DNA kit. DNA libraries were then multiplexed and sequenced on a NextSeq2000 (Paired End; P2 – 100 cycles). For data analysis, quality and adapter filtering was applied to raw reads using ‘trim_galore’ before aligning to mouse assembly mm9 with bowtie2 using the default parameters. The Picard tool MarkDuplicates (http://broadinstitute.github.io/picard/) was used to remove reads with the same start site and

orientation. The BEDTools suite (http://bedtools.readthedocs.io) was used to create read density profiles. Enriched regions were discovered using MACS2[44] and scored against matched input libraries (fold change > 2 and FDR-adjusted p-value < 0.1). A consensus peak atlas was then created by filtering out blacklisted regions (http://mitra.stanford.edu/kundaje/akundaje/release/blacklists/mm9-mouse/mm9-blacklist.bed.gz) and then merging all peaks within 500 bp. A raw count matrix was computed over this atlas using featureCounts[39] with the '-p' option for fragment counting. The count matrix and all genome browser tracks were normalized to a sequencing depth of ten million mapped fragments. DESeq2[45] was used to classify differential peaks between two conditions using fold change > 2 and FDR-adjusted p-value < 0.1. Peak-gene associations were made using linear genomic distance to the nearest transcription start site with Homer.[46]

CUT&TAG.—Following pancreas cell isolation, one tube of 100k DAPI-/tdTomato+ acinar cells were sorted into FACS buffer supplemented with FBS for each CUT&TAG reaction. CUT&Tag data was carried out following the methods outlined by Henikoff and colleagues.[47] Data were analysed using the nf-core/cutandrun pipeline v3.0[48]. In brief, reads were aligned to the mouse genome (mm9) using bowtie2 v2.4.4[49], duplicate reads were removed with Picard v2.27.4, and peak calling was performing using SEACR v1.3[40] with 'norm' and 'stringent' parameters. Consensus peak sets were created with the R package DiffBind v3.4.11[51], and differentially modified regions were detected with DESeq2 v1.34.0 (FDR < 0.05)[45]. Peaks were annotated with ChIPseeker::annotatePeak v1.30.3[52] with respect to Gencode vM1 annotations.

Single-cell ATAC-sequencing.—Data was processed using the 10X Genomics cellranger-ARC v1.0.0 pipeline for demultiplexing and alignment. The resulting output from cellranger-ARC was further analyzed in R using the ArchR v1.0.2 package.[53] Cells were filtered based on sequencing depth and signal-to-noise ratio: cells with fewer than 10^3.4 unique fragments and a TSS enrichment ratio outside the range of 10 to 35 were discarded. Doublet enrichment was computed using ArchR's addDoubletScores function (default parameters), followed by doublet filtering with the filterDoublets function (filterRatio=1). Differentially accessible peaks identified from the bulk ATAC-seq were quantified using the addPeakSet and addPeakMatrix functions. An iterative latent semantic indexing (LSI) dimensionality reduction was performed using this peak matrix with ArchR's addIterativeLSI function, with 2 iterations and a resolution of 0.2. Clustering was performed using ArchR's addClusters function with a resolution of 0.8. Finally, ArchR's addUMAP function was used to compute a UMAP embedding with 30 nearest neighbors and a minimum distance of 0.5.

Acinar 3D cell culture preparation.—Following isolation of acinar cells, cell pellets were resuspended in acinar-explant (AE) media composed of DMEM supplemented with 1% FBS, 1% PS, 1% STI and then mixed with Matrigel (Corning) in a 2:1 ratio cells:Matrigel. Per 24- well plate, 400 µl of the cells:Matrigel suspension were plated and incubated at 37 °C for solidification for at least 1 hour. Upon Matrigel solidification, 400 µl of warm AE media was added with or without TGF-α at 50ng/ml concentration. Media (with and without TGF-α) was changed at day 1 and day 3 of culture. Brightfield image

at 4X and 10X magnification were taken using a Nikon ECLIPSE Ti inverted microscope system equipped with an Andor Zyla 5.5 sCMOS camera.

Analysis of brightfield images of spheroids with computer vision.—Images were acquired in OME-TIFF format with 16-bit depth in grayscale. Illumination was normalized by subtracting the image passed by a gaussian filter of sigma = 5 * max(x_dim, y_dim) / 300, where x/y_dim are the image dimensions. Images were then inverted and intensity values clipped to the intensity between 3 and 99.8 percentiles, scaling image intensity values to unit range. To segment the spheroid objects from the background, we detected edges in the image by Sobel filtering, and seeded the watershed algorithm using values below 0.3 as background and above 0.95 as positive. We dilated objects in this binary mask with a disk of 3 pixels of diameter, and filtered objects smaller than 32 pixels in diameter. We removed further smaller objects by applying closing (dilation followed by erosion), filling holes within objects, and applying erosion and dilation again, all with a 3 pixel diameter disk. All operations were performed using scikit-image version 0.18.2.11 We then quantified various features for each object in each image using the skimage.measure.regionprops function, and reduced values per image using the mean. Statistical testing was performed between groups of interest with a two-sided Mann–Whitney U test, and adjusted for multiple comparisons with the Benjamini–Hochberg False Discovery Rate method using pingouin (version 0.4.0).[54]

Histopathology and immunofluorescence staining.—Pancreata were fixed overnight in 4% buffered PFA, transferred to 70% ethanol, and then embedded in paraffin using IDEXX BioAnalytics laboratory. Serial sections were cut and hematoxylin and eosin (H&E) staining performed. For IF, slides were deparaffinized, underwent an antigen retrieval using Sodium citrate buffer, blocked with 5% BSA supplemented with 0.4% Triton X-100 in PBS, and primary antibodies were incubated overnight at 4°C. Secondary antibodies conjugated with Alexa-488 or Alexa-647 (Invitrogen) were used and DAPI nuclear counterstaining was performed. Fluorescent images were captured with a Nikon ECLIPSE Ti inverted microscope system equipped with an Andor Zyla 5.5 sCMOS camera. For Alcian blue staining, we used the Alcian Blue (ph2.5) Stain Kit (#H-3501) following the manufacturer's recommendation. H&E and Alcian blue images were captured with a ZEISS Axio Scope.A1 equipped with a Axiocam 105 color and analyzed using ImageJ.

Flow cytometry preparation and analysis.—A single cell suspension was generated, and red blood cells (RBCs) removed by using the ACK RBC lysis buffer. Cell suspensions were then stained for extracellular markers (after live/dead staining with Zombie Aqua) per the manufacturer's instructions, using primary antibodies conjugated to fluorophores in FACS buffer containing 2% FBS. After washing, cells were resuspended in FACS buffer (2% FBS), and analyzed on an Attune NxT flow cytometer. Data analyses were performed with FlowJo software.

Single-cell RNA-sequencing.—A single cell suspension was generated and subjected to 10x Chromium scRNA-seq as per the manufacturer's instruction. Analysis was performed using Seurat methods.[55] Briefly, raw sequencing data files were preprocessed (e.g.

demultiplexed cellular barcodes, read alignment, and generation of gene count matrix) using the Cell Ranger Single Cell Software Suite provided by 10x Genomics. The feature matrix generated by Cell Ranger was used to perform downstream analysis using R toolkit Seurat. Quality control filters were used to exclude low-quality cells. The first filter assessed the level of mitochondrial RNA content in each cell—cells with <10% mitochondrial RNA passed the filter. Then, the presence of outliers (e.g. doublets and low detection cells) were determined by evaluating the distribution of cells given the levels of unique RNA transcript number and total RNA transcript numbers—aberrantly high gene count (doublets/multiplets); low gene diversity (low-quality cells/empty droplets). Parameters were set to include cells with gene number values below 4000 and above 800. A filtered Seurat object was subsequently created with high confidence cells that have passed the threshold tests implemented above. Seurat was also implemented for subsequent downstream analyses. To generate a 2-dimensional plot visualizing the different single-cell clusters, default parameters were set for the Uniform Manifold Approximation and Projection (UMAP) method.

Gene set enrichment analysis.—Using normalized read counts of RNA-seq data, the fgseaMultilevel function from the fgsea package with the following parameters were used: minGSSize = 15; maxGSSize = 500 MSigDB Hallmark, MSigDB KEGG, MSigDB REACTOME, and MSigDB Biocarta gene sets were tested for all analyses. Genes were ranked based on DESeq's wald statistic (stat), which takes into account the log-fold change and its standard error.

Quantification and statistical analysis.

The number of animals is based on feasibility considerations and our interest in observing a relatively large effect size. In addition, a power analysis was performed with a desired power of 0.8, $\alpha = 0.05$, and a literature search was performed to find expected averages and standard deviations based on similar protocols. Tests for differences between two groups were performed using two-tailed unpaired Student t test or two-tailed Mann–Whitney test, or for three or more groups by one-way ANOVA, as specified in the figure legends. P values were considered significant if less than 0.05. All graphs depict mean ± SEM unless otherwise indicated. The exact value of number of replicates (n) is indicated in the figure legends and refers to number of animals or biological replicates, as indicated. Asterisks used to indicate significance correspond with *, $P < 0.05$; **, $P < 0.01$; ***, $P < 0.001$; ****, $P < 0.0001$. GraphPad Prism 9 (GraphPad Software) was used for statistical analysis of experiments, data processing, and presentation.

Supplementary Material

Refer to Web version on PubMed Central for supplementary material.

ACKNOWLEDGMENTS

We thank L. Dow, S. Josefowicz, R. Niec, E. Piskounova, J. Pitarresi, and A. Rustgi for critical readings of the manuscript. This work was supported by NIDDK R01DK060694 (RC), AACR-PanCAN Pathway to Leadership Award (RC), Emerson Collective Cancer Research Fund (RC), American Surgical Association Fellowship Award

(RC). DJF is supported by a NIH/NCI Ruth L. Kirschstein NRSA F31CA265166; AG by the Prevent Cancer Foundation; AFR by a NCI T32CA203702 grant.

REFERENCES

1. Foster SL, Hargreaves DC, and Medzhitov R (2007). Gene-specific control of inflammation by TLR-induced chromatin modifications. Nature, 447, 972–978. doi: 10.1038/nature05836. [PubMed: 17538624]
2. Ostuni R, Piccolo V, Barozzi I, Polletti S, Termanini A, Bonifacio S, Curina A, Prosperini E, Ghisletti S, and Natoli G (2013). Latent enhancers activated by stimulation in differentiated cells. Cell, 152, 157–171. doi: 10.1016/j.cell.2012.12.018. [PubMed: 23332752]
3. Naik S, Larsen SB, Gomez NC, Alaverdyan K, Sendoel A, Yuan S, Polak L, Kulukian A, Chai S, Fuchs E (2017). Inflammatory memory sensitizes skin epithelial stem cells to tissue damage. Nature 550, 475–480. doi: 10.1038/nature24271. [PubMed: 29045388]
4. Ordovas-Montanes J, Dwyer DF, Nyquist SK, Buchheit KM, Vukovic M, Deb C, Wadsworth MH 2nd, Hughes TK, Kazer SW, Yoshimoto E, et al. (2018). Allergic inflammatory memory in human respiratory epithelial progenitor cells. Nature 560, 649–654. doi: 10.1038/s41586-018-0449-8. [PubMed: 30135581]
5. Means AL, Meszoely IM, Suzuki K, Miyamoto Y, Rustgi AK, Coffey RJ Jr., Wright CV, Stoffers DA, Leach SD (2005). Pancreatic epithelial plasticity mediated by acinar cell transdifferentiation and generation of nestin-positive intermediates. Development 132, 3767–3776. doi: 10.1242/dev.01925. [PubMed: 16020518]
6. Fendrich V, Esni F, Garay MV, Feldmann G, Habbe N, Jensen JN, Dor Y, Stoffers D, Jensen J, Leach SD, et al. (2008). Hedgehog signaling is required for effective regeneration of exocrine pancreas. Gastroenterology 135, 621–631. doi: 10.1053/j.gastro.2008.04.011. [PubMed: 18515092]
7. Kopp JL, Dubois CL, Hao E, Thorel F, Herrera PL, Sander M (2011). Progenitor cell domains in the developing and adult pancreas. Cell Cycle 10, 1921–1927. doi: 10.4161/cc.10.12.16010. [PubMed: 21558806]
8. Grimont A, Leach SD, Chandwani R (2021). Uncertain Beginnings: Acinar and Ductal Cell Plasticity in the Development of Pancreatic Cancer. Cell Mol Gastroenterol Hepatol 13, 369–382. doi: 10.1016/j.jcmgh.2021.07.014. [PubMed: 34352406]
9. Guerra C, Schuhmacher AJ, Cañamero M, Grippo PJ, Verdaguer L, Pérez-Gallego L, Dubus P, Sandgren EP, Barbacid M (2007). Chronic pancreatitis is essential for induction of pancreatic ductal adenocarcinoma by K-Ras oncogenes in adult mice. Cancer Cell 11, 291–302. doi: 10.1016/j.ccr.2007.01.012. [PubMed: 17349585]
10. Guerra C, Collado M, Navas C, Schuhmacher AJ, Hernández-Porras I, Cañamero M, Rodriguez-Justo M, Serrano M, Barbacid M (2011). Pancreatitis-induced inflammation contributes to pancreatic cancer by inhibiting oncogene-induced senescence. Cancer Cell 19, 728–739. doi: 10.1016/j.ccr.2011.05.011. [PubMed: 21665147]
11. Habbe N, Shi G, Meguid RA, Fendrich V, Esni F, Chen H, Feldmann G, Stoffers DA, Konieczny SF, Leach SD, et al. (2008). Spontaneous induction of murine pancreatic intraepithelial neoplasia (mPanIN) by acinar cell targeting of oncogenic Kras in adult mice. Proc Natl Acad Sci U S A 105, 18913–18918. doi: 10.1073/pnas.0810097105. [PubMed: 19028870]
12. Kopp JL, von Figura G, Mayes E, Liu FF, Dubois CL, Morris JP 4th, Pan FC, Akiyama H, Wright CV, Jensen K, et al. (2012). Identification of Sox9-dependent acinar-to-ductal reprogramming as the principal mechanism for initiation of pancreatic ductal adenocarcinoma. Cancer Cell 22, 737–750. doi: 10.1016/j.ccr.2012.10.025. [PubMed: 23201164]
13. Cobo I, Martinelli P, Flández M, Bakiri L, Zhang M, Carrillo-de-Santa-Pau E, Jia J, Sánchez-Arévalo Lobo VJ, Megías D, Felipe I, et al. (2018). Transcriptional regulation by NR5A2 links differentiation and inflammation in the pancreas. Nature 554, 533–537. doi: 10.1038/nature25751. [PubMed: 29443959]
14. Alonso-Curbelo D, Ho YJ, Burdziak C, Maag JLV, Morris JP 4th, Chandwani R, Chen HA, Tsanov KM, Barriga FM, Luan W, et al. (2021). A gene-environment-induced epigenetic program initiates tumorigenesis. Nature 590, 642–648. doi: 10.1038/s41586-020-03147-x. [PubMed: 33536616]

15. Li Y, He Y, Peng J, Su Z, Li Z, Zhang B, Ma J, Zhuo M, Zou D, Liu X, et al. (2021). Mutant Kras co-opts a proto-oncogenic enhancer network in inflammation-induced metaplastic progenitor cells to initiate pancreatic cancer. Nat Cancer 2, 49–65. doi: 10.1038/s43018-020-00134-z. [PubMed: 35121887]

16. Westphalen CB, Takemoto Y, Tanaka T, Macchini M, Jiang Z, Renz BW, Chen X, Ormanns S, Nagar K, Tailor Y, et al. (2016). Dclk1 Defines Quiescent Pancreatic Progenitors that Promote Injury-Induced Regeneration and Tumorigenesis. Cell Stem Cell 18, 441–455. doi: 10.1016/j.stem.2016.03.016. [PubMed: 27058937]

17. Kirkegård J, Cronin-Fenton D, Heide-Jørgensen U, Mortensen FV (2018). Acute Pancreatitis and Pancreatic Cancer Risk: A Nationwide Matched-Cohort Study in Denmark. Gastroenterology 154, 1729–1736. doi: 10.1053/j.gastro.2018.02.011. [PubMed: 29432727]

18. Del Poggetto E, Ho IL, Balestrieri C, Yen EY, Zhang S, Citron F, Shah R, Corti D, Diaferia GR, Li CY, et al. (2021). Epithelial memory of inflammation limits tissue damage while promoting pancreatic tumorigenesis. Science 373, eabj0486. doi: 10.1126/science.abj0486. [PubMed: 34529467]

19. Larsen SB, Cowley CJ, Sajjath SM, Barrows D, Yang Y, Carroll TS, Fuchs E (2021). Establishment, maintenance, and recall of inflammatory memory. Cell Stem Cell 28, 1758–1774.e8. doi: 10.1016/j.stem.2021.07.001. [PubMed: 34320411]

20. Schlesinger Y, Yosefov-Levi O, Kolodkin-Gal D, Granit RZ, Peters L, Kalifa R, Xia L, Nasereddin A, Shiff I, Amran O, et al. (2020). Single-cell transcriptomes of pancreatic preinvasive lesions and cancer reveal acinar metaplastic cells' heterogeneity. Nat Commun 11, 4516. doi: 10.1038/s41467-020-18207-z. [PubMed: 32908137]

21. Shi G, DiRenzo D, Qu C, Barney D, Miley D, Konieczny SF (2013). Maintenance of acinar cell organization is critical to preventing Kras-induced acinar-ductal metaplasia. Oncogene 32(15), 1950–1958. doi: 10.1038/onc.2012.210. [PubMed: 22665051]

22. Liou GY, Döppler H, Necela B, Krishna M, Crawford HC, Raimondo M, Storz P (2013). Macrophage-secreted cytokines drive pancreatic acinar-to-ductal metaplasia through NF-κB and MMPs. J Cell Biol 202(3), 563–577. doi: 10.1083/jcb.201301001. [PubMed: 23918941]

23. Zhang Y, Yan W, Mathew E, Kane KT, Brannon A 3rd, Adoumie M, Vinta A, Crawford HC, Pasca di Magliano M (2017). Epithelial-Myeloid cell crosstalk regulates acinar cell plasticity and pancreatic remodeling in mice. Elife 6, e27388. doi: 10.7554/eLife.27388. [PubMed: 28980940]

24. Liu X, Pitarresi JR, Cuitiño MC, Kladney RD, Woelke SA, Sizemore GM, Nayak SG, Egriboz O, Schweickert PG, Yu L, et al. (2016). Genetic ablation of Smoothened in pancreatic fibroblasts increases acinar-ductal metaplasia. Genes Dev 30(17), 1943–1955. doi: 10.1101/gad.283499.116. [PubMed: 27633013]

25. McAllister F, Bailey JM, Alsina J, Nirschl CJ, Sharma R, Fan H, Rattigan Y, Roeser JC, Lankapalli RH, Zhang H, et al. (2014). Oncogenic Kras activates a hematopoietic-to-epithelial IL-17 signaling axis in preinvasive pancreatic neoplasia. Cancer Cell 25, 621–637. doi: 10.1016/j.ccr.2014.03.014. [PubMed: 24823639]

26. Reichert M, Takano S, von Burstin J, Kim SB, Lee JS, Ihida-Stansbury K, Hahn C, Heeg S, Schneider G, Rhim AD, et al. The Prrx1 homeodomain transcription factor plays a central role in pancreatic regeneration and carcinogenesis. Genes Dev 27, 288–300. doi: 10.1101/gad.204453.112.

27. Jadhav U, Cavazza A, Banerjee KK, Xie H, O'Neill NK, Saenz-Vash V, Herbert Z, Madha S, Orkin SH, Zhai H, et al. (2019). Extensive Recovery of Embryonic Enhancer and Gene Memory Stored in Hypomethylated Enhancer DNA. Mol Cell 74, 542–554.e5. doi: 10.1016/j.molcel.2019.02.024. [PubMed: 30905509]

28. Gonzales KAU, Polak L, Matos I, Tierney MT, Gola A, Wong E, Infarinato NR, Nikolova M, Luo S, Liu S, et al. (2021). Stem cells expand potency and alter tissue fitness by accumulating diverse epigenetic memories. Science 374, eabh2444. doi: 10.1126/science.abh2444. [PubMed: 34822296]

29. Ying H, Kimmelman AC, Lyssiotis CA, Hua S, Chu GC, Fletcher-Sananikone E, Locasale JW, Son J, Zhang H, Coloff JL, et al. (2012). Oncogenic Kras maintains pancreatic tumors through regulation of anabolic glucose metabolism. Cell 149, 656–670. doi: 10.1016/j.cell.2012.01.058. [PubMed: 22541435]

30. Collins MA, Bednar F, Zhang Y, Brisset JC, Galbán S, Galbán CJ, Rakshit S, Flannagan KS, Adsay NV, Pasca di Magliano M (2012). Oncogenic Kras is required for both the initiation and maintenance of pancreatic cancer in mice. J Clin Invest 122, 639–653. doi: 10.1172/JCI59227. [PubMed: 22232209]

31. Halbrook CJ, Wen HJ, Ruggeri JM, Takeuchi KK, Zhang Y, di Magliano MP, Crawford HC (2017). Mitogen-activated Protein Kinase Kinase Activity Maintains Acinar-to-Ductal Metaplasia and Is Required for Organ Regeneration in Pancreatitis. Cell Mol Gastroenterol Hepatol 3, 99–118. doi: 10.1016/j.jcmgh.2016.09.009. [PubMed: 28090569]

32. Lau CM, Adams NM, Geary CD, Weizman OE, Rapp M, Pritykin Y, Leslie CS, Sun JC (2018). Epigenetic control of innate and adaptive immune memory. Nat Immunol, 19, 963–972. doi: 10.1038/s41590-018-0176-1. [PubMed: 30082830]

33. de Laval B, Maurizio J, Kandalla PK, Brisou G, Simonnet L, Huber C, Gimenez G, Matcovitch-Natan O, Reinhardt S, David E, et al. (2020). C/EBPβ-Dependent Epigenetic Memory Induces Trained Immunity in Hematopoietic Stem Cells. Cell Stem Cell 26, 657–674.e8. doi: 10.1016/j.stem.2020.01.017. [PubMed: 32169166]

34. Jackson EL, Willis N, Mercer K, Bronson RT, Crowley D, Montoya R, Jacks T, Tuveson DA (2001). Analysis of lung tumor initiation and progression using conditional expression of oncogenic K-ras. Genes Dev 15, 3243–3248. doi: 10.1101/gad.943001. [PubMed: 11751630]

35. Tuveson DA, Shaw AT, Willis NA, Silver DP, Jackson EL, Chang S, Mercer KL, Grochow R, Hock H, Crowley D, et al. (2004). Endogenous oncogenic K-ras(G12D) stimulates proliferation and widespread neoplastic and developmental defects. Cancer Cell 5, 375–387. doi: 10.1016/s1535-6108(04)00085-6. [PubMed: 15093544]

36. Madisen L, Zwingman TA, Sunkin SM, Oh SW, Zariwala HA, Gu H, Ng LL, Palmiter RD, Hawrylycz MJ, Jones AR, et al. (2010). A robust and high-throughput Cre reporting and characterization system for the whole mouse brain. Nat Neurosci 13, 133–140. doi: 10.1038/nn.2467. [PubMed: 20023653]

37. Dobin A, Davis CA, Schlesinger F, Drenkow J, Zaleski C, Jha S, Batut P, Chaisson M, Gingeras TR (2013). STAR: ultrafast universal RNA-seq aligner. Bioinformatics 29, 15–21. doi: 10.1093/bioinformatics/bts635. [PubMed: 23104886]

38. Harrow J, Frankish A, Gonzalez JM, Tapanari E, Diekhans M, Kokocinski F, Aken BL, Barrell D, Zadissa A, Searle S, et al. (2012). GENCODE: the reference human genome annotation for The ENCODE Project. Genome Res 22, 1760–1774. doi: 10.1101/gr.135350.111. [PubMed: 22955987]

39. Liao Y, Smyth GK, Shi W (2014). featureCounts: an efficient general purpose program for assigning sequence reads to genomic features. Bioinformatics 30, 923–930. doi: 10.1093/bioinformatics/btt656. [PubMed: 24227677]

40. Wingett SW, Andrews S (2018). FastQ Screen: A tool for multi-genome mapping and quality control. F1000Res 7, 1338. doi: 10.12688/f1000research.15931.2. [PubMed: 30254741]

41. Hartley SW, Mullikin JC (2015). QoRTs: a comprehensive toolset for quality control and data processing of RNA-Seq experiments. BMC Bioinformatics 16, 224. doi: 10.1186/s12859-015-0670-5. [PubMed: 26187896]

42. Law CW, Chen Y, Shi W, Smyth GK (2014). voom: Precision weights unlock linear model analysis tools for RNA-seq read counts. Genome Biol 15, R29. doi: 10.1186/gb-2014-15-2-r29. [PubMed: 24485249]

43. Buenrostro JD, Giresi PG, Zaba LC, Chang HY, Greenleaf WJ (2013). Transposition of native chromatin for fast and sensitive epigenomic profiling of open chromatin, DNA-binding proteins and nucleosome position. Nat Methods 10, 1213–1218. doi: 10.1038/nmeth.2688. [PubMed: 24097267]

44. Zhang Y, Liu T, Meyer CA, Eeckhoute J, Johnson DS, Bernstein BE, Nusbaum C, Myers RM, Brown M, Li W, et al. (2008). Model-based analysis of ChIP-Seq (MACS). Genome biology 9, R137. doi: 10.1186/gb-2008-9-9-r137 [PubMed: 18798982]

45. Love MI, Huber W, and Anders S (2014). Moderated estimation of fold change and dispersion for RNA-seq data with DESeq2. Genome biology 15, 550. doi: 10.1186/s13059-014-0550-8. [PubMed: 25516281]

46. Heinz S, Benner C, Spann N, Bertolino E, Lin YC, Laslo P, Cheng JX, Murre C, Singh H, Glass CK (2010). Simple combinations of lineage-determining transcription factors prime cis-regulatory elements required for macrophage and B cell identities. Mol Cell 38, 576–589. doi: 10.1016/j.molcel.2010.05.004 [PubMed: 20513432]
47. Kaya-Okur HS, Janssens DH, Henikoff JG, Ahmad K, Henikoff S (2020). Efficient low-cost chromatin profiling with CUT&Tag. Nat Protoc 15, 3264–3283. doi: 10.1038/s41596-020-0373-x. [PubMed: 32913232]
48. Ewels PA, Peltzer A, Fillinger S, Patel H, Alneberg J, Wilm A, Garcia MU, Di Tommaso P, and Nahnsen S (2020). The nf-core framework for community-curated bioinformatics pipelines. Nat Biotech 38, 276–278. doi: 10.1038/s41587-020-0439-x.
49. Langmead B, and Salzberg SL (2012). Fast gapped-read alignment with Bowtie 2. Nature Methods 9, 357–359. doi: 10.1038/nmeth.1923. [PubMed: 22388286]
50. Meers MP, Tenenbaum D, and Henikoff S (2019). Peak calling by Sparse Enrichment Analysis for CUT&RUN chromatin profiling. Epigenetics & Chromatin 12, 42. doi: 10.1186/s13072-019-0287-4. [PubMed: 31300027]
51. Ross-Innes CS, Stark R, Teschendorff AE, Holmes KA, Ali HR, Dunning MJ, Brown GD, Gojis O, Ellis IO, Green AR, et al. (2012). Differential oestrogen receptor binding is associated with clinical outcome in breast cancer. Nature 481, 389–393. doi: 10.1038/nature10730. [PubMed: 22217937]
52. Yu G, Wang LG, and He QY (2015). ChIPseeker: an R/Bioconductor package for ChIP peak annotation, comparison and visualization. Bioinformatics 31, 2382–2383. doi: 10.1093/bioinformatics/btv145. [PubMed: 25765347]
53. Granja JM, Corces MR, Pierce SE, Bagdatli ST, Choudhry H, Chang HY, and Greenleaf WJ (2021). ArchR is a scalable software package for integrative single-cell chromatin accessibility analysis. Nat Genetics 53, 403–411. doi: 10.1038/s41588-021-00790-6. [PubMed: 33633365]
54. Vallat R (2018). Pingouin: statistics in Python. J. Open Source Softw 3, 1026. doi: 10.21105/joss.01026.
55. Stuart T, Butler A, Hoffman P, Hafemeister C, Papalexi E, Mauck WM 3rd, Hao Y, Stoeckius M, Smibert P, Satija R (2019). Comprehensive Integration of Single-Cell Data. Cell 177, 1888–1902.e21. doi: 10.1016/j.cell.2019.05.031. [PubMed: 31178118]

Highlights

- Inflammation is durably encoded as epigenetic alterations in pancreatic acinar cells
- Lineage-specific epithelial memory represents an incomplete cell fate decision
- Memory controls lineage plasticity and can be recalled by oncogenic Kras
- Inflammatory memory is reversible as a potential cancer prevention strategy

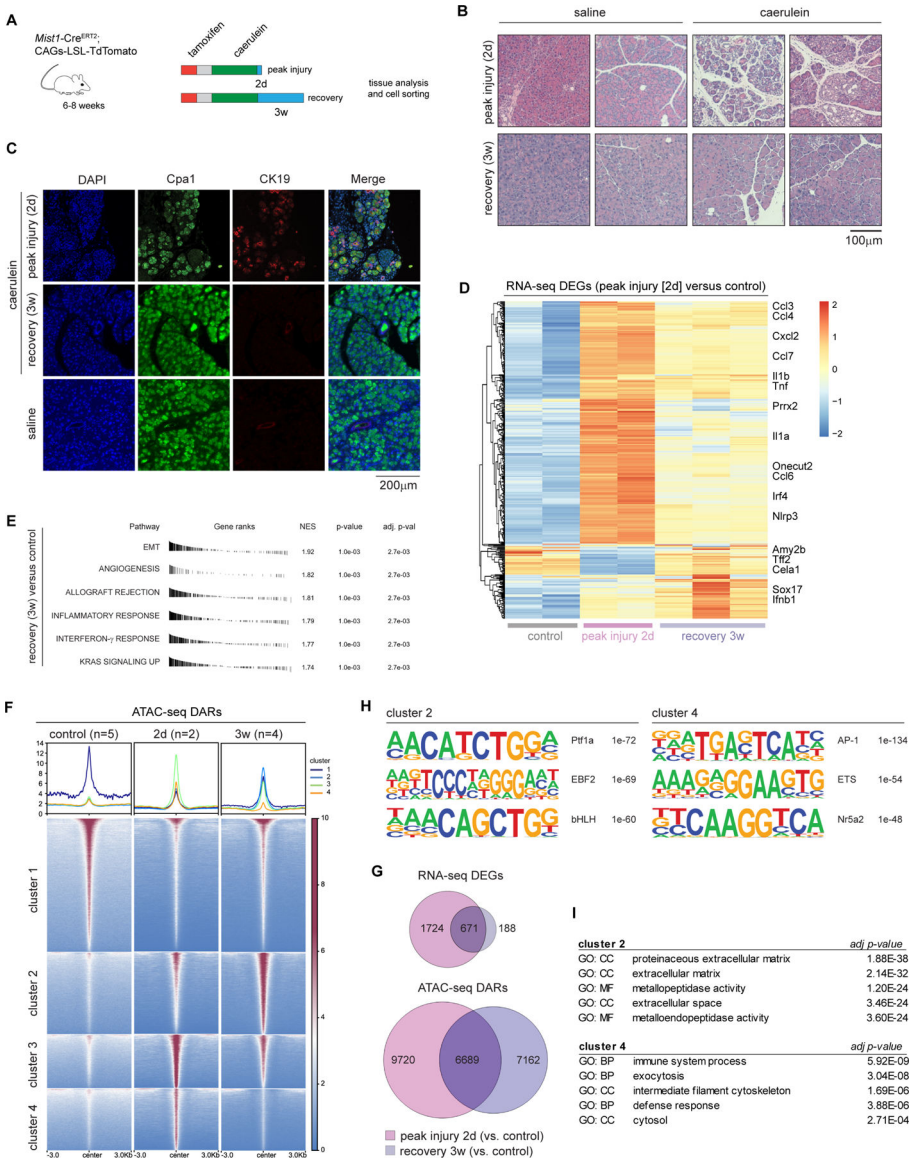

Figure 1. A transient inflammatory episode induces persistent molecular alterations following pancreatic regeneration.

A, Schematic representation of lineage-traced mouse model. **B**, Representative hematoxylin/eosin staining of mouse pancreas sections following caerulein-induced pancreatitis. **C**, Immunofluorescence staining of pancreas sections for DAPI, tdTomato, Carboxypeptidase A1 (Cpa1), and Cytokeratin 19 (CK19). Images are representative of N=3 mice/condition. **D**, Heatmap of RNA-seq data identifying 417 differentially expressed genes (thresholds: [log2(fold change)]>1; $p_{adj} < 0.01$) when comparing naïve tdTomato(+) (control) and peak injury tdTomato(+) acinar cells (recovery 2d); supervised clustering according to indicated condition. Each column is a biological replicate mouse. **E**, Gene Set Enrichment Analysis (GSEA) of RNA-seq data between control and recovery 3w condition, top six results are shown. NES = normalized enrichment score. **F**, Tornado plots of differentially accessible chromatin generated with k-means cluster analysis across all pairwise contrasts. Each column represents the average signal across N=2–5 biological replicate mice. **G**, Venn

diagrams illustrating the degree of overlap between 2 days of recovery versus control and 3 weeks of recovery versus control from a transcriptional (top) and chromatin accessibility (bottom) standpoint; log2FC>1; FDR<0.05. **H**, HOMER analysis depicting top three motif enrichments in Cluster 2 and Cluster 4. **I**, GO term enrichment for differentially accessible sites in Cluster 2 and Cluster 4. Top five results are shown. CC=cellular component; BP=biological process; MF=molecular function.

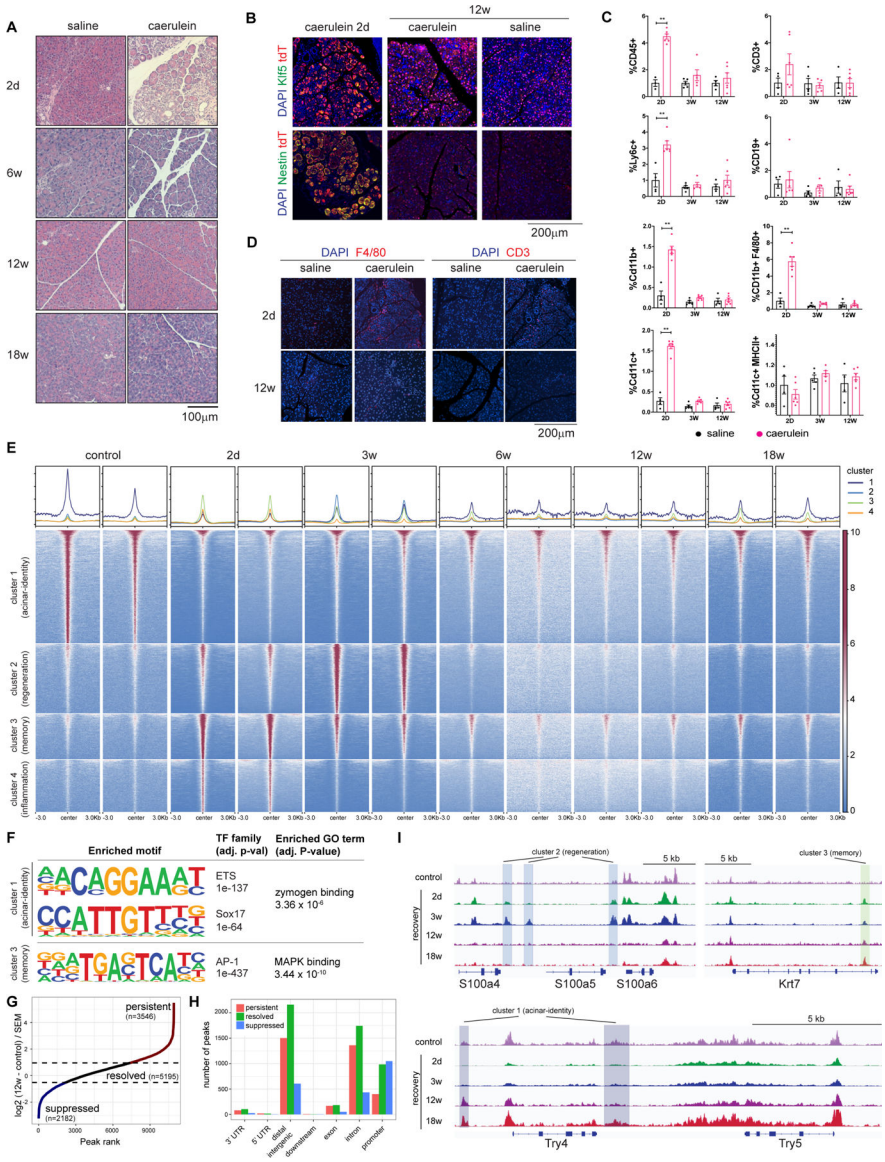

Figure 2. An epigenetic of memory of inflammatory injury is durable over time.

A, Representative hematoxylin/eosin staining of naïve (saline) or prior injury (caerulein-treated) mouse pancreas sections. **B**, Immunofluorescence staining of pancreas sections for Cpa1, tdTomato, Klf5, Nestin and DAPI 2 days and 12 weeks after pancreatitis (or control). Representative images shown are from a total of N=2–5 mice per condition. **C**, Flow cytometric quantification of CD45(+), CD3(+), Ly6c(+), CD19(+), CD11b(+), CD11b(+) F4/80(+), CD11c(+), and CD11c(+) MHCII(+) immune cell populations in the pancreata of naïve (saline) and injury-exposed (caerulein) mice. Student's t-test was performed between conditions. N=3–5 mice per condition. **D**, Immunofluorescence staining in pancreas sections for F4/80, CD3 and DAPI 2 days and 12 weeks after pancreatitis. **E**, Tornado plots of differentially accessible chromatin generated with k-means cluster analysis across all pairwise contrasts. Each column represents the average signal across N=2–5 biological replicate mice. **F**, HOMER analysis depicting motif enrichment in Cluster 1 and Cluster

3 and the top GO term. **G**, ELBOW plot of all differentially accessible regions that gain accessibility in caerulein-treated tdTomato(+) acinar cells collected at the peak of injury (n = 10,924 peaks) ranked by their Wald statistic in samples collected after 12 weeks of recovery (log2 fold change/SEM). SEM, standard error of the mean. **H**, Bar plot quantifying the number of peak injury 2d UP peaks, categorized on the basis of ELBOW analysis that overlap with genomic annotations. **I**, Genome browser traces of ATAC signal from tdTomato(+) acinar cells collected from mice treated with either saline or caerulein and collected after 2 days, 3 weeks, 12 weeks, or 18 weeks of recovery. Scale bar 0–60.

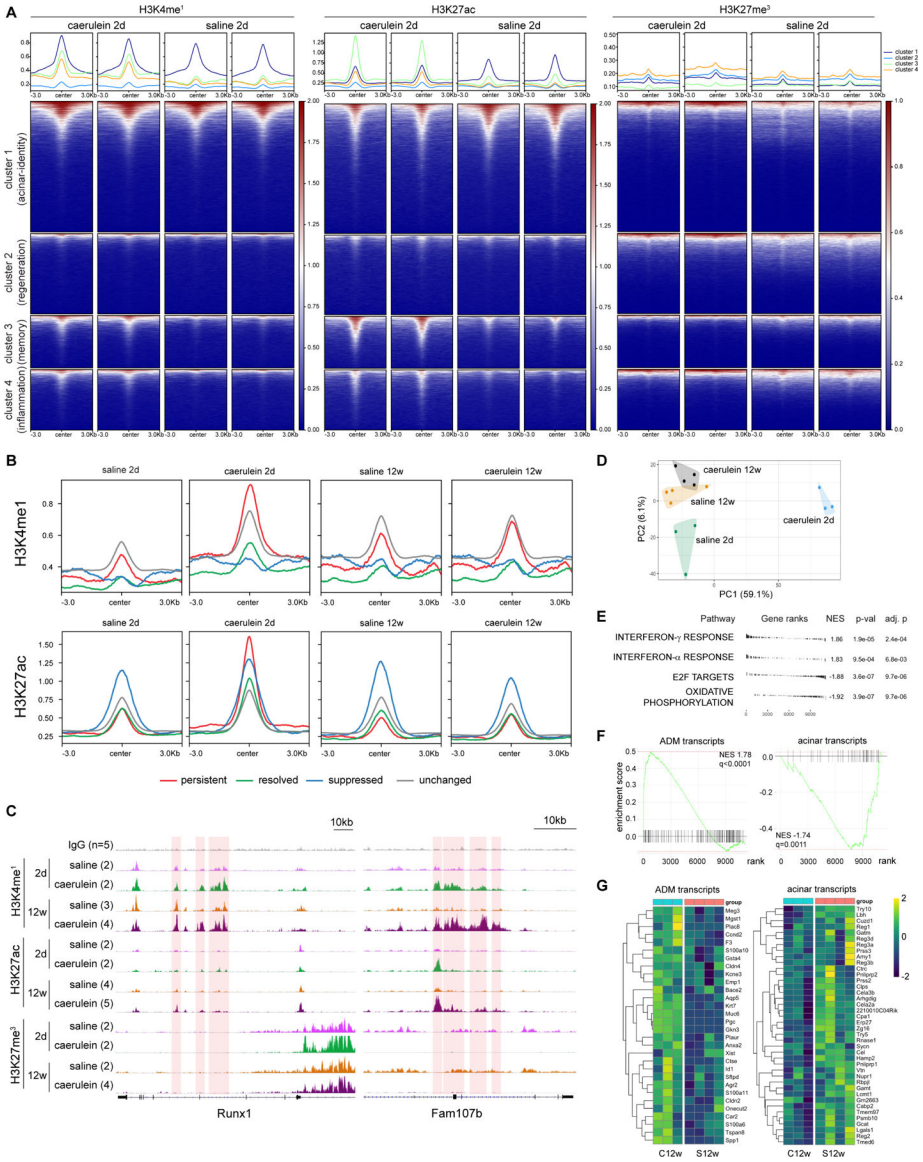

Figure 3. Memory of inflammatory injury features retention of H3K4me^1 and manifests as an 'incomplete cell fate decision'

A, Signal intensity traces and tornado plots of the histone modifications H3K4me1, H3K27ac, and H3K27me3 generated with CUT&TAG data at clusters 1/2/3/4 (as in Figure 1F). **B**, Signal intensity traces of H3K4me1 and H3K27ac localization at peak injury 2d UP ATAC-seq peaks categorized on the basis of ELBOW analysis. **C**, IGV traces of genomic loci with overlay of CUT&TAG signals from tdTomato(+) acinar cells (n=2–5 mice per condition) treated with either saline or caerulein and collected after 2 days and 12 weeks of recovery. Vertical rectangular boxes indicate persistent ATAC peaks as determined by ELBOW. Scale bars: IgG (0–10); H3K4me^1 (0–7); H3K27ac (0–15); H3K27me^3 (0–5). **D**, Principal Component Analysis (PCA) plot of bulk RNA-seq data generated from tdTomato(+) acinar cells collected 2 days and 12 weeks after either pancreatitis or control treatment. **E-F,** GSEA of RNA-seq data derived from naïve tdTomato(+) acinar cells versus injury-exposed tdTomato(+) acinar cells (12 weeks of recovery). **E,** Top 4 most up- or down-

regulated Hallmarks are shown. **F**, Indicated ADM and acinar gene sets.[20] NES=normalized enrichment score. **G**, Heatmap of RNA-seq data delineating the leading edge ADM and acinar transcripts in C12w and S12w samples; each column represents a biological replicate mouse.

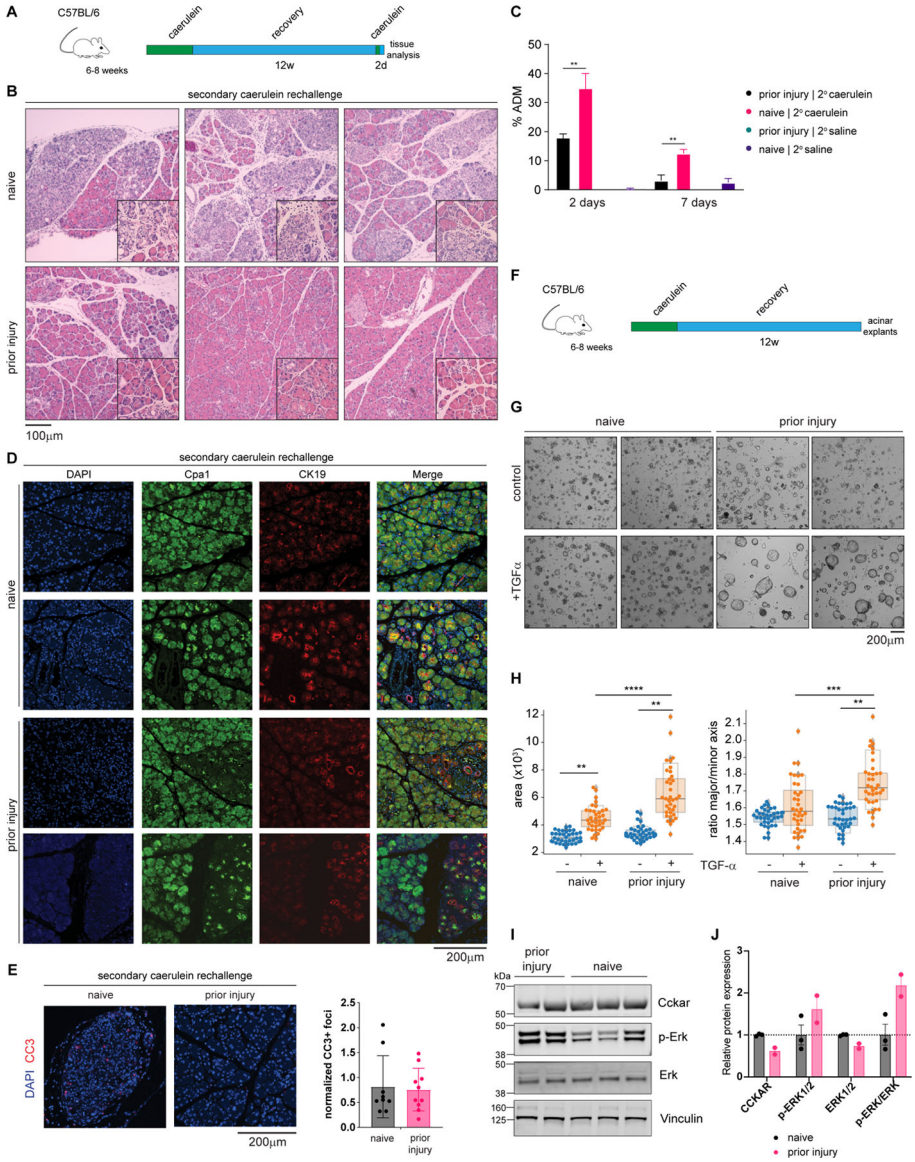

Figure 4. Prior inflammatory injury alters the capacity for subsequent metaplasia.

A, Schematic representation of primary pancreatitis and inflammatory re-challenge treatment regimen in wild-type mice. **B**, Hematoxylin/eosin staining of naïve (N=4) and injury-resolved (N=5) mouse pancreas sections collected 2 days after inflammatory re-challenge. **C**, Quantification of the ADM area in the pancreas of naïve and injury-resolved mice re-challenged with either saline or caerulein (n=3–5/condition). Student's t-test was performed. **D**, Immunofluorescence for Cpa1 and CK19 and DAPI in naïve and injury-resolved mouse pancreas sections collected 2 days after inflammatory re-challenge. Representative images of N=2–5 mice per condition. **E**, Representative immunofluorescence for cleaved caspase 3 (CC3) and DAPI staining of naïve and injury-resolved pancreas sections collected 2 days after inflammatory re-challenge. Representative images of N=2–5 mice per condition. **F**, Schematic representation of primary pancreatitis followed by prolonged recovery and acinar explant generation. **G**, Representative images of acinar

explants generated from naïve and injury-resolved mice; N=4 mice/condition. **H**, Boxplots of image analysis of naïve and injury-resolved explants treated with vehicle or recombinant human TGFα. Each point represents an object in one of 3 wells per mouse, N=4 mice per condition. Mann-Whitney was performed. **I**, Western blot of bulk pancreas tissue lysate extracted from naive and injury-resolved mice at 12w of recovery. **J**, Quantification of **I**.

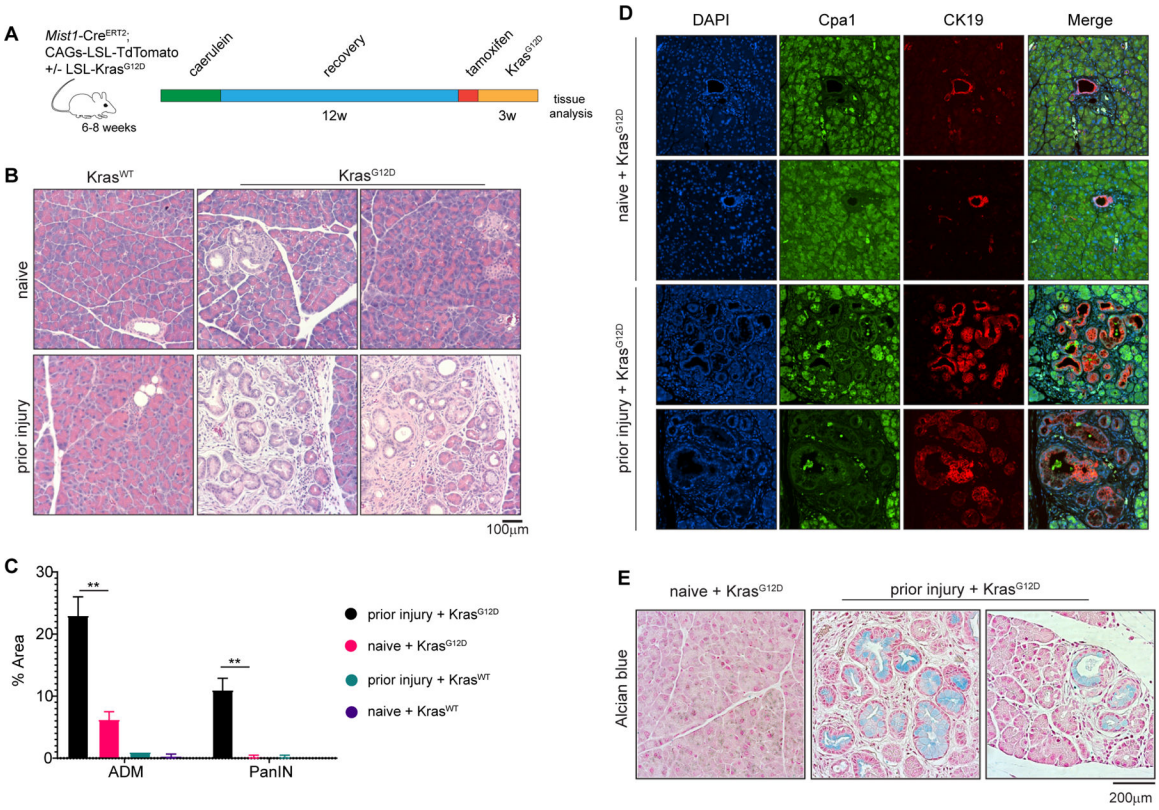

Figure 5. Prior inflammatory injury lowers the threshold for subsequent Kras-driven tumor initiation.

A, Schematic representation of lineage-traced mouse model with initial exposure to pancreatitis, prolonged recovery, and delayed Kras^{G12D} activation. **B**, Hematoxylin/eosin staining of naïve and injury-exposed mouse pancreas sections collected after 12 weeks of recovery and 3 weeks of mutant Kras activation. Representative images of N=4–5 mice per condition. **C**, Histologic quantification of ADM and PanIN lesions in pancreas collected from mice exposed to the corresponding conditions wherein duration of Kras^{G12D} activation is 3 weeks. **D**, Immunofluorescence for Cpa1 and CK19 and DAPI staining of pancreas sections collected from naïve and injury-resolved mice exposed to 12 weeks of recovery and then 3 weeks of mutant Kras. Representative images of N=2–5 mice per condition. **E**, Alcian blue staining of pancreas sections collected from naïve and injury-resolved mice after 12 weeks of recovery and then 3 weeks of Kras^{G12D}. Images are representative of N=4–5 mice per condition.

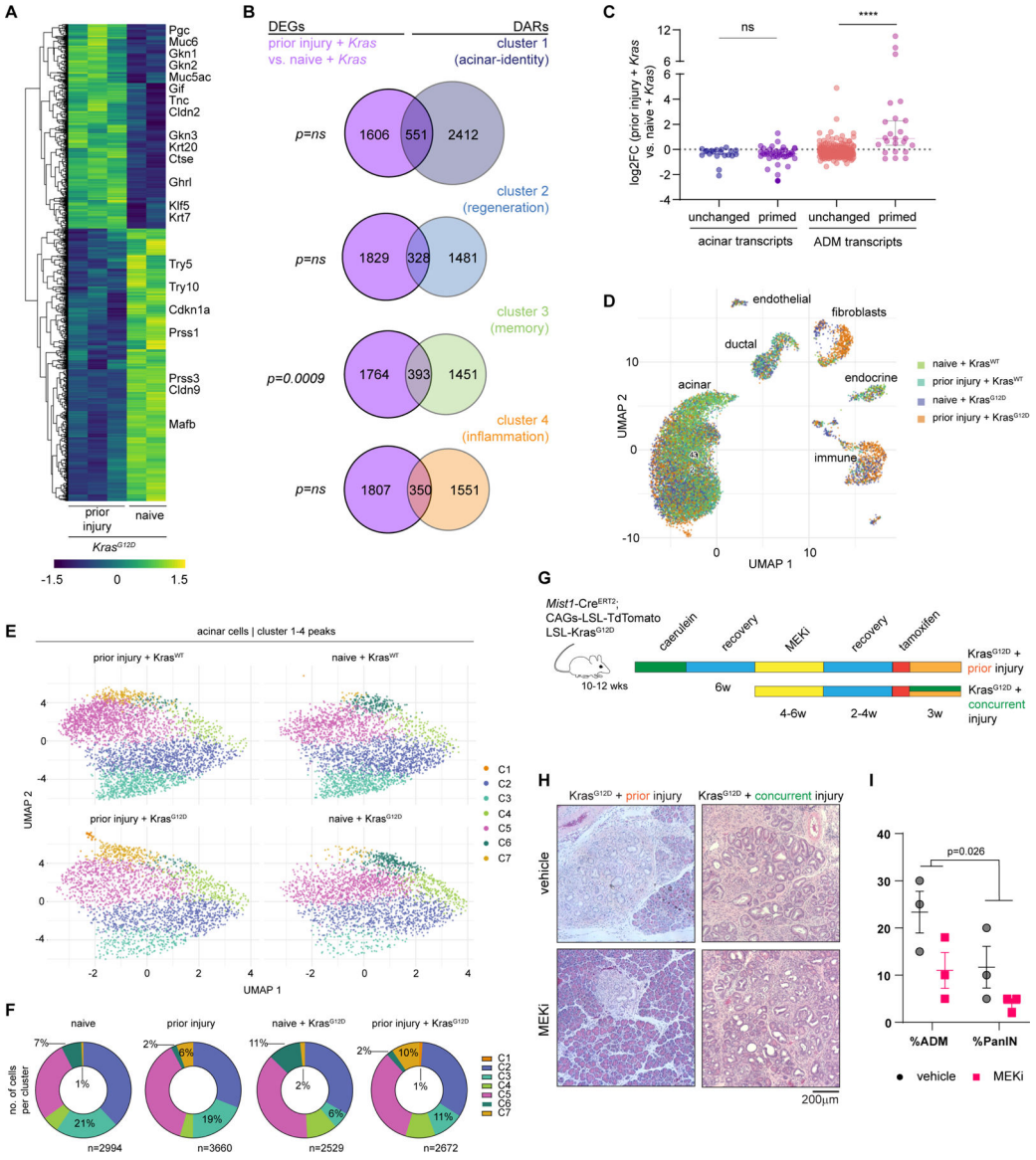

Figure 6. An epigenetic memory of prior injury is recalled in the response to mutant *Kras* and can be reversed by MAPK pathway inhibition.

A, Heatmap of differentially expressed genes between naïve and injury-resolved tdTomato(+) acinar cells after 12 weeks of recovery and then 2 days of $Kras^{G12D}$. Threshold of p_{adj}<0.1 was used to identify DEGs. **B**, Venn diagrams illustrating the degree of overlap between differentially expressed genes (DEGs) altered with prior caerulein plus brief $Kras^{G12D}$ activation and genes associated with differentially accessible regions (DARs) enriched in respective clusters. Fisher's exact test was used. **C**, Dot plot illustrating the fold change of leading edge 'acinar transcripts' (primed) and leading edge 'ADM transcripts' (primed) compared to unchanged 'acinar transcripts' and unchanged 'ADM transcripts' (identified from Figure 2I–J) in naïve and injury-resolved tdTomato(+) acinar cells exposed to 12 weeks of recovery and then 2 days of $Kras^{G12D}$. Student's t-test was performed to compare conditions. **D**, UMAP of single-cell ATAC-seq data from naïve and injury-resolved mice exposed to 12 weeks of recovery before and after 2 days of $Kras^{G12D}$. **E**, Split UMAP

of pancreatic epithelial cells on the basis of clusters 1/2/3/4 peaks (as defined in Figure 1F). **F**, Quantification of pancreatic epithelial cell abundance in samples exposed to either saline or caerulein followed by 12 weeks of recovery +/− $Kras^{G12D}$. **G**, Schematic representation of lineage-traced mouse model treated with MEK inhibitor during recovery from caerulein. **H**, Representative hematoxylin/eosin staining of pancreas sections as per treatment in **G**. **I,** Quantification of the ADM and PanIN area of pancreas sections (N=3 per condition) shown in **H**. Two-way ANOVA was performed to compare conditions.

Key resources table

REAGENT or RESOURCE	SOURCE	IDENTIFIER
Antibodies		
Rabbit Polyclonal anti-Sox9	Millipore	Cat# AB5535, RRID:AB_2239761
Rabbit Polyclonal anti-mCherry	Abcam	Cat# ab167453, RRID:AB_2571870
Rabbit Monoclonal anti-CD3	Abcam	Cat# ab16669, RRID:AB_443425
Chicken Polyclonal anti-mCherry	Abcam	Cat# ab205402, RRID:AB_2722769
Rabbit Monoclonal anti-F4/80	Cell Signaling Technology	Cat# 70076, RRID:AB_2799771
Goat Polyclonal anti-KLF4	R&D Systems	Cat# AF3158, RRID:AB_2130245
Goat Polyclonal anti-KLF5	R&D Systems	Cat# AF3758, RRID:AB_2130246
Rabbit Polyclonal anti-Nestin	Sigma-Aldrich	Cat# N5413, RRID:AB_1841032
Rabbit Polyclonal anti-RFP	Rockland	Cat# 600-401-379, RRID:AB_2209751
Rabbit Monoclonal anti-DCAMKL1 (Dclk1)	Abcam	Cat# ab109029, RRID:AB_10864128
Goat Polyclonal Anti-Mouse Carboxypeptidase A1	R&D Systems	Cat# AF2765, RRID:AB_2085841
Rabbit Monoclonal anti-Cytokeratin 19	Abcam	Cat# ab52625, RRID:AB_2281020
Phospho-p44/42 MAPK (Erk1/2) (Thr202/Tyr204)	Cell Signaling Technology	Cat# 4370S RRID:AB_2315112
Goat Polyclonal anti-Chicken IgY H&L (Alexa Fluor® 488)	Abcam	Cat# ab150169, RRID:AB_2636803
Goat Polyclonal anti-Mouse IgY H&L (Alexa Fluor® 488)	Abcam	Cat# ab150113, RRID:AB_2576208
Goat Polyclonal Anti-Mouse IgG H&L (Alexa Fluor 647) Antibody	Abcam	Cat# ab150115, RRID:AB_2687948
Rat Monoclonal anti-mouse CD3 coupled with Alexa Fluor(R) 700	BioLegend	Cat# 100216, RRID:AB_493697
Armenian hamster Monoclonal anti-mouse CD11c coupled with Pacific Blue(TM)	BioLegend	Cat# 117321, RRID:AB_755987
Rat Monoclonal anti-mouse F4/80 coupled with Brilliant Violet 605(TM)	BioLegend	Cat# 123133, RRID:AB_2562305
Rat Monoclonal anti-mouse CD19 coupled with Brilliant Violet 711(TM)	BioLegend	Cat# 115555, RRID:AB_2565970
Rat Monoclonal anti-mouse Ly-6C coupled with PE	BioLegend	Cat# 128007, RRID:AB_1186133
Rat Monoclonal anti-mouse I-A/I-E coupled with APC	BioLegend	Cat# 107613, RRID:AB_313328
Rat Monoclonal anti-mouse CD45 coupled with PE/Cyanine7	BioLegend	Cat# 103113, RRID:AB_312978
Rat Monoclonal anti-mouse CD11b coupled with APC/Cyanine7	BioLegend	Cat# 101225, RRID:AB_830641
Rat Monoclonal anti-mouse CD3 coupled with APC/Cyanine7	BioLegend	Cat# 100221, RRID:AB_2057374
Rat Monoclonal anti-mouse CD19 coupled with PerCP/Cyanine5.5	BioLegend	Cat# 152405, RRID:AB_2629814
Anti-Vinculin antibody [EPR8185] (ab129002)	Abcam	ab129002
CCKAR Polyclonal Antibody	Thermo Fisher Scientific	BS-11514R
P44/42 MAPK (Erk1/2) (137F5) Rabbit mAb	Cell Signaling Technology	4695S
CUTANA™ pAG-Tn5 for ChIC/CUT&Tag	EpiCypher	15-1017

REAGENT or RESOURCE	SOURCE	IDENTIFIER
CUTANA® High Fidelity 2X PCR Master Mix for CUT&Tag	EpiCypher	15-1018
Rabbit IgG An5body, CUTANA™ CUT&RUN Nega5ve Control	EpiCypher	13-0042
An5-Rabbit Secondary An5body for CUTANA™ ChIC/CUT&Tag Workflows	EpiCypher	13-0047
CUTANA™ E. coli Spike-in DNA	EpiCypher	18-1401
Anti-Mouse Secondary Antibody for CUTANA™ ChIC/CUT&Tag Workflows	EpiCypher	13-0048
CUTANA® Concanavalin A Conjugated Paramagnetic Beads	EpiCypher	21-1401
Histone H3K27ac Antibody, SNAP-ChIP Certified	EpiCypher	13-0045
Histone H3K4me1 Antibody, SNAP-ChIP Certified	EpiCypher	13-0040
H3K27me3 Monoclonal Antibody (G.299.10), ChIP-Verified	ThermoFisher Scientific	MA5-11198
Acetyl-Histone H3 (Lys27) Monoclonal Antibody, Unconjugated, Species Reactivity: Human, Host: Mouse / IgG1	ThermoFisherScientific	MA5-23516
Chemicals, peptides, and recombinant proteins		
Deoxyribonuclease I from bovine pancreas	Sigma-Aldrich	DN25-100MG
Collagenase from Clostridium	Sigma-Aldrich	C9263-500MG
Collagenase D	Sigma-Aldrich	11088882001
Dispase, neutral protease grade II	Roche	4942078001
Trypsin inhibtor from Glycine max (soybean)	Sigma-Aldrich	T9003-250MG
Tamoxifen	Sigma-Aldrich	T5648-5G
Corn oil	Sigma-Aldrich	C8267-500ML
20% Paraformaldehyde Aqueous Solution, EM Grade	Electron Microscopy Sciences	15713-S
Histo-Clear II	National Diagnostics	HS2021GLL
EGTA (Ethylene glycol-bis(2-aminoethylether)-N,N,N′,N′-tetraacetic acid)	Sigma-Aldrich	E3889-100G
TRIzol LS Reagent	Invitrogen	10296028
Recombinant Human TGFalpha	R&D Systems	239-A-100
ACK lysing buffer	ThermoFisher Scientific	A1049201
Caerulein	Bachem	4030451.0005
Matrigel Matrix	Corning	356231
Dexamethasone	Sigma-Aldrich	D8893-1MG
DAPI (4’,6-Diamidino-2-Phenylindole, Dilactate)	ThermoFisher Scientific	Cat# D3571, RRID:AB_2307445
TDE1 Tagment DNA Enzyme and TD Buffer	Illumina	20034198
Trametinib diet (5mg/kg)	Bio-Serv	S10136
Zombie Aqua Fixable Viability Kit 100 tests	BioLegend	423101
Critical commercial assays		
Agilent High Sensitivity DNA kit	Agilent	5067-4626
MinElute PCR Purification Kit	Qiagen	28006

REAGENT or RESOURCE	SOURCE	IDENTIFIER
Alcian Blue (pH 2.5) Stain Kit	Vector Laboratories	H-3501
Agilent RNA 6000 Nano Kit	Agilent	5067-1511
Deposited data		
Raw and analyzed data (scRNA-seq; bulk RNA-seq; ATAC-seq)	This paper	GEO: GSE198564
Mouse reference genome assembly MGSCv37 (mm9)	Genome Reference Consortium	http://www.ncbi.nlm.nih.gov/projects/genome/assembly/grc/mouse/
Experimental models: Organisms/strains		
Mouse: Mist1:CreERT2	The Jackson Laboratory	RRID:IMSR_JAX:029228
Mouse: LSL-KrasG12D	The Jackson Laboratory	RRID:IMSR_JAX:008179
Mouse: LSL-tdTomato	The Jackson Laboratory	RRID:IMSR_JAX:007909
Mouse: C57BL/6J	The Jackson Laboratory	RRID:IMSR_JAX:000664
Oligonucleotides		
Primers for Genotyping		
Mist1 common forward	Integrated DNA Technologies	GGT TTA AGC AAA TTG TCA AGT ACG G
Mist1 reverse	Integrated DNA Technologies	ATA GTA AGT ATG GTG GCG GTC AGC G
Mist1-Cre ER reverse	Integrated DNA Technologies	GAA GCA TTT TCC AGG TAT GCT CAG
Kras1	Integrated DNA Technologies	GTC TTT CCC CAG CAC AGT GC
Kras2	Integrated DNA Technologies	CTC TTG CCT ACG CCA CCA GCT C
Kras3	Integrated DNA Technologies	AGC TAG CCA CCA TGG CTT GAG TAA GTC TGC A
CAG-Tdtomato Tg FP	Integrated DNA Technologies	CTG TTC CTG TAC GGC ATG G
CAG-Tdtomato Tg RP	Integrated DNA Technologies	GGC ATT AAA GCA GCG TAT CC
CAG-Tdtomato wt FP	Integrated DNA Technologies	AAG GGA GCT GCA GTG GAG TA
CAG-Tdtomato wt RP	Integrated DNA Technologies	CCG AAA ATC TGT GGG AAG TC
Software and algorithms		
STAR	Dobin et al.37	https://github.com/alexdobin/STAR
Gencode vM1	Harrow et al.38	https://www.gencodegenes.org/mouse/
featureCounts	Liao et al.39	http://subread.sourceforge.net/
FastQC	Wingett et al.40	https://github.com/s-andrews/FastQC
QoRTs	Hartley et al.41	https://hartleys.github.io/QoRTs/
limma voom	Law et al.42	https://rdrr.io/bioc/limma/man/voom.html
Picard	Broad Institute	https://broadinstitute.github.io/picard/
MarkDuplicates	Broad Institute	http://broadinstitute.github.io/picard/
BEDTools suite	Quinlan laboratory at the University of Utah	http://bedtools.readthedocs.io
MACS2	Zhang et al.44	https://github.com/macs3-project/MACS
DESeq2	Love et al.[45]	https://bioconductor.org/packages/release/bioc/html/DESeq2.html
HOMER	Heinz et al.[46]	http://homer.ucsd.edu

REAGENT or RESOURCE	SOURCE	IDENTIFIER
Nf-core CutAndRun Pipeline	Ewels et al.48	https://www.biorxiv.org/content/10.1101/610741v3
Bowtie2	Langmead and Salzberg.49	http://bowtie-bio.sourceforge.net/bowtie2/index.shtml
SEACR	Meers et al.50	http://seacr.fredhutch.org/
DiffBind	Ross-Innes et al.51	https://www.nature.com/articles/nature10730
ChIPseeker	Yu et al.[52]	https://academic.oup.com/bioinformatics/article/31/14/2382/255379?login=true
ArchR	Granja et al.53	https://www.nature.com/articles/s41588-021-00790-6
Scikit-Image	van der Walt and colleagues	https://scikit-image.org/
ImageJ	NIH	https://imagej.nih.gov/ij/
Seurat	Stuart et al.[55]	https://www.satijalab.org/seurat
Cell Ranger	10x Genomics	http://10xgenomics.com
GraphPad Prism 9	GraphPad Software	https://www.graphpad.com/
Adobe Illustrator 2022	Adobe	https://www.adobe.com/
FlowJo Software	BD	https://www.flowjo.com/
Integrative Genomics Viewer	Broad Institute	https://software.broadinstitute.org/software/igv/